Cell Reports
Medicine

Article

A bispecific antibody targeting EGFR and AXL delays resistance to osimertinib

Graphical abstract

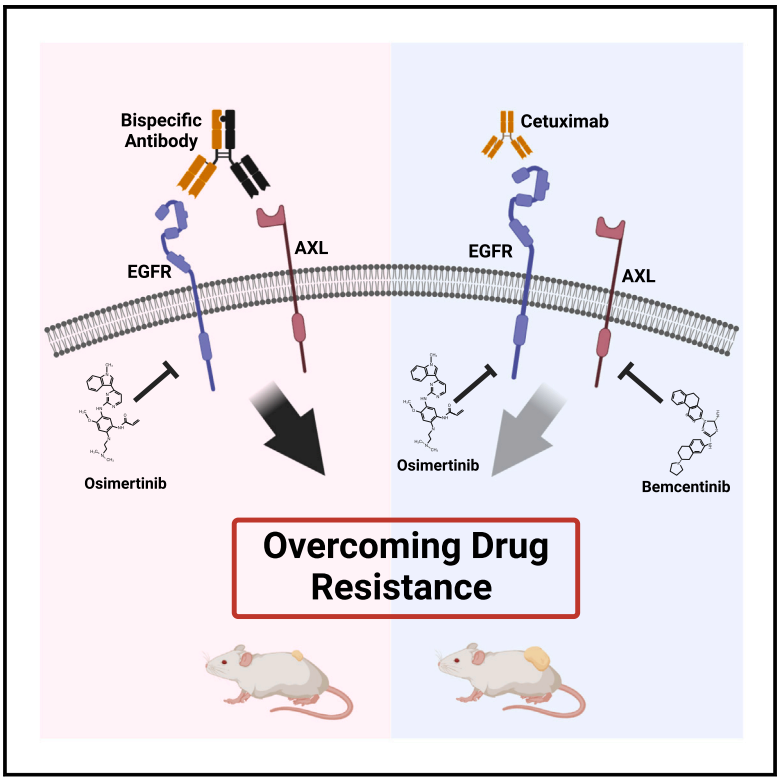

Highlights

- Kinase inhibitors (KIs) can block EGFR-positive NSCLC but relapses limit drug efficacy
- Blocking AXL better delays relapses if anti-AXL antibodies, not KIs, are used
- Combining a KI and a bispecific antibody engaging AXL and EGFR delays relapses in mice

Authors

Arturo Simoni-Nieves, Moshit Lindzen, Suvendu Giri, ..., Mattia Lauriola, Ilaria Marrocco, Yosef Yarden

Correspondence

ilaria.marrocco@unicatt.it (I.M.), yosef.yarden@weizmann.ac.il (Y.Y.)

In brief

Simoni-Nieves et al. combine an EGFR kinase inhibitor (osimertinib) and a bispecific antibody co-inhibiting AXL and EGFR to block relapses of EGFR-mutated lung cancer models. This combination exceeds the efficacy achieved by other drug combinations, including osimertinib plus an AXL-specific kinase inhibitor.

Simoni-Nieves et al., 2024, Cell Reports Medicine *5*, 101703
September 17, 2024
https://doi.org/10.1016/j.xcrm.2024.101703

CellPress

Please cite this article in press as: Simoni-Nieves et al., A bispecific antibody targeting EGFR and AXL delays resistance to osimertinib, Cell Reports Medicine (2024), https://doi.org/10.1016/j.xcrm.2024.101703

Cell Reports Medicine

CellPress
OPEN ACCESS

Article

A bispecific antibody targeting EGFR and AXL delays resistance to osimertinib

Arturo Simoni-Nieves,[1,9] Moshit Lindzen,[1,9] Suvendu Giri,[1] Nitin Gupta,[1] Rishita Chatterjee,[1] Boobash-Raj Selvadurai,[1] Marieke Van Daele,[1] Danielle Love,[1] Yuya Haga,[2] Donatella Romaniello,[3] Tomer-Meir Salame,[4] Mirie Zerbib,[5] Roni Oren,[5] Yasuo Tsutsumi,[2,6,7] Mattia Lauriola,[3] Ilaria Marrocco,[8,*] and Yosef Yarden[1,10,*]

[1]Departments of Immunology and Regenerative Biology, Weizmann Institute of Science, Rehovot 76100, Israel
[2]Graduate School of Pharmaceutical Sciences, Osaka University, Osaka 565-0871, Japan
[3]Department of Medical and Surgical Sciences (DIMEC), University of Bologna, 40126 Bologna, Italy
[4]Flow Cytometry Unit, Life Sciences Core Facilities, Weizmann Institute of Science, Rehovot 76100, Israel
[5]Department of Veterinary Resources, Weizmann Institute of Science, Rehovot 76100, Israel
[6]Global Center for Medical Engineering and Informatics, Osaka University, Osaka 565-0871, Japan
[7]Institute for Open and Transdisciplinary Research Initiatives, Osaka University, Osaka 565-0871, Japan
[8]Department of Life Sciences and Public Health, Università Cattolica del Sacro Cuore, 00168 Rome, Italy
[9]These authors contributed equally
[10]Lead contact
*Correspondence: ilaria.marrocco@unicatt.it (I.M.), yosef.yarden@weizmann.ac.il (Y.Y.)
https://doi.org/10.1016/j.xcrm.2024.101703

SUMMARY

Activating EGFR (epidermal growth factor receptor) mutations can be inhibited by specific tyrosine kinase inhibitors (TKIs), which have changed the landscape of lung cancer therapy. However, due to secondary mutations and bypass receptors, such as AXL (AXL receptor tyrosine kinase), drug resistance eventually emerges in most patients treated with the first-, second-, or third-generation TKIs (e.g., osimertinib). To inhibit AXL and resistance to osimertinib, we compare two anti-AXL drugs, an antibody (mAb654) and a TKI (bemcentinib). While no pair of osimertinib and an anti-AXL drug is able to prevent relapses, triplets combining osimertinib, cetuximab (an anti-EGFR antibody), and either anti-AXL drug are initially effective. However, longer monitoring uncovers superiority of the mAb654-containing triplet, possibly due to induction of receptor endocytosis, activation of immune mechanisms, or disabling intrinsic mutators. Hence, we constructed a bispecific antibody that engages both AXL and EGFR. When combined with osimertinib, the bispecific antibody consistently inhibits tumor relapses, which warrants clinical trials.

INTRODUCTION

The major histological type of lung cancer, non-small cell lung cancer (NSCLC), includes three subtypes, of which adenocarcinoma is the most common and the one that frequently presents actionable mutations (e.g., in *KRAS*, *EGFR*, and *BRAF*[1]). Although immune checkpoint blockers (ICBs) benefit a fraction of patients with metastatic NSCLC, such as the *KRAS*- and *BRAF*-mutated NSCLC,[2] tumors expressing the common mutant forms of EGFR poorly respond to ICBs.[3] In contrast, the corresponding patients well respond to ATP-competitive EGFR inhibitors.[4–6] However, nearly all treated patients evolve resistance to the tyrosine kinase inhibitors (TKIs). The T790M mutation is the major driver of acquired resistance to the non-covalent EGFR inhibitors.[7] Other mechanisms include upregulation of compensatory signaling pathways and the upstream receptors, such as AXL,[8] *HER2*,[9] and either the neuregulin-HER3 axis[10] or the route instigated by the hepatocyte growth factor (HGF) and the cognate receptor, MET.[11,12] Third-generation TKIs, such as osimertinib, specifically inhibit EGFR-T790M by means of irreversible binding with cysteine 797. Clinical trials that compared osimertinib and chemotherapy[13] or osimertinib and standard EGFR-specific TKIs[14] led to the approval of osimertinib for patients who progressed following TKI treatment and also for treatment-naive patients. Unfortunately, a variety of mechanisms permit secondary resistance to osimertinib, including emergence of C797S mutation.[15–17]

It is imperative differentiating between two classes of EGFR mutations: (1) short deletions in exon 19 (Del19) or a point mutation (L858R),[18] and several less frequent pioneering mutations,[19] and (ii) the T790M and C797S secondary mutations.[7,20–22] Whereas the primary mutations slowly accumulate in normal tissues,[23] the mechanisms underlying the rapid emergence of secondary mutations are incompletely understood. In analogy to bacteria exposed to antibiotics, which activate the SOS mutagenic response,[24] mammalian cells exposed to TKIs initially undergo epigenetic alterations that select rare drug-tolerant persister (DTP) cells[25] characterized by altered energy consumption.[26] These reversible events are likely followed by the

Please cite this article in press as: Simoni-Nieves et al., A bispecific antibody targeting EGFR and AXL delays resistance to osimertinib, Cell Reports Medicine (2024), https://doi.org/10.1016/j.xcrm.2024.101703

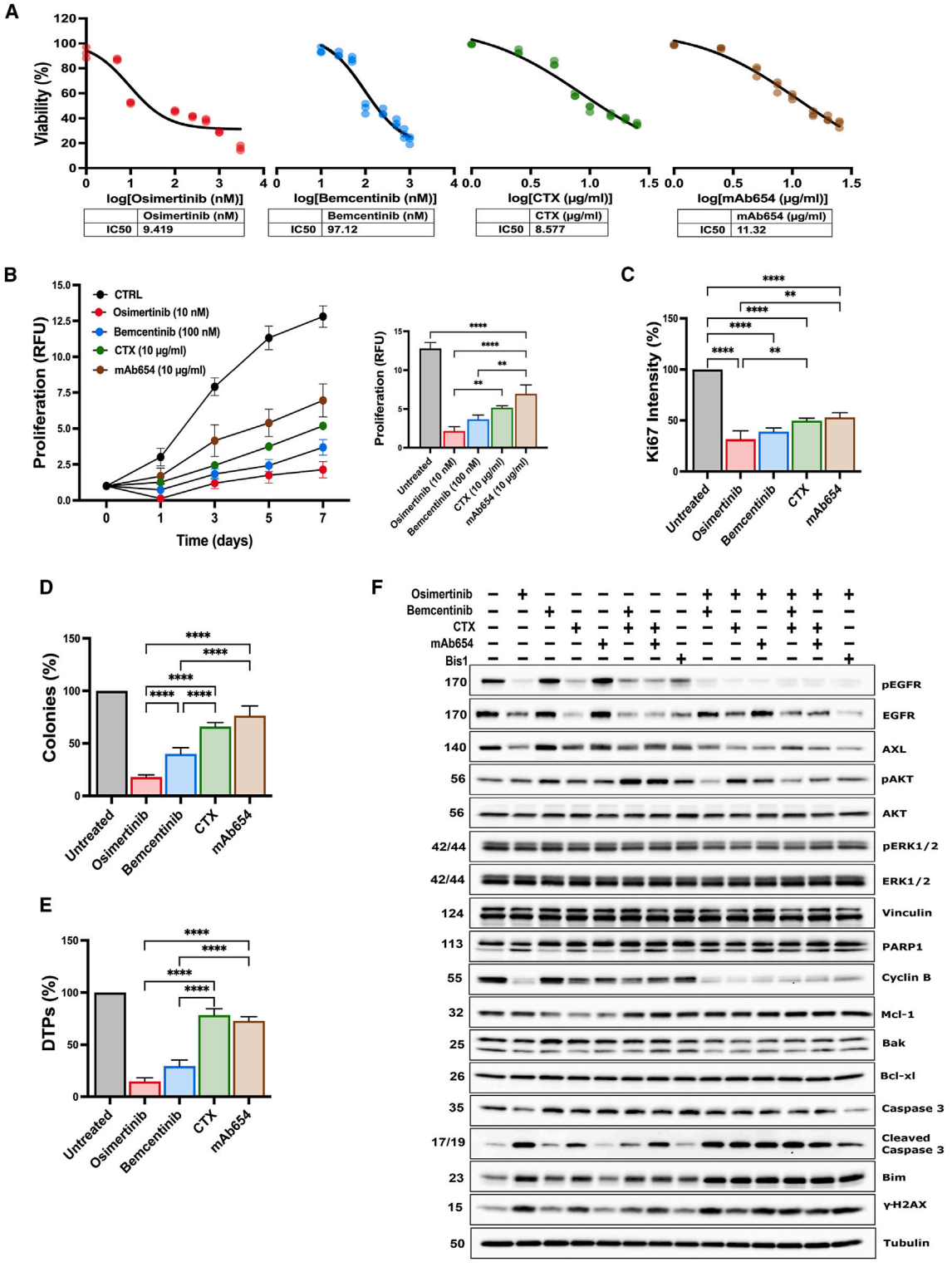

Figure 1. *In vitro* effects of single anti-EGFR and anti-AXL drugs

(A) PC9 cells (3×10^3) were seeded in 96-well plates and later treated for 72 h with increasing concentrations of cetuximab, mAb654, bemcentinib, or osimertinib. Cell viability was assessed using the MTT (3-(4,5-dimethylthiazol-2-yl)-2,5-diphenyltetrazolium bromide) assay.

(B) PC9 cells were seeded in 96-well plates (1,000 cells/well), and on the next day they were treated for 7 days with CTX (10 μg/mL), mAb654 (10 μg/mL), bemcentinib (100 nM), or osimertinib (10 nM). Thereafter, cells were fixed and stained with crystal violet. Data are shown as means ± SEM of three experiments.

(legend continued on next page)

Please cite this article in press as: Simoni-Nieves et al., A bispecific antibody targeting EGFR and AXL delays resistance to osimertinib, Cell Reports Medicine (2024), https://doi.org/10.1016/j.xcrm.2024.101703

SOS-like response that blocks DNA repair and generates mutations. The endogenous mutators comprise a group of low-fidelity DNA polymerases.[27] Because activation of bypass pathways permits drug resistance, simultaneous inhibition of EGFR and bypass receptors is considered a logical therapeutic strategy.[28] Indeed, antibody-based co-inhibition of EGFR, HER2, and/or HER3 demonstrated activity in animal models.[29–33] In the same vein, amivantamab, a bispecific antibody (bsAb) co-targeting MET and EGFR, has been approved for patients expressing EGFR with exon 20 insertions.[34] In similarity to other receptors, AXL is involved in DTP generation,[35,36] and experimental therapies involving EGFR-specific TKIs and either an AXL-specific TKI[37,38] or an AXL-specific monoclonal antibody (mAb)[27] were able to prevent resistance in NSCLC models.

Many individual TKI resistance mechanisms coalesce into recruitment of a parallel pathway.[39] While such evasion mechanisms require simultaneous application of a second drug, whether or not the type of the second drug, a mAb or a TKI, can dictate treatment outcome is currently unresolved. Herein we studied resistance to osimertinib and found that overcoming resistance requires co-administration of osimertinib, cetuximab (an anti-EGFR mAb), and an inhibitor of AXL, either an antibody (mAb654) or a TKI (bemcentinib). Systematic analyses of the biological effects of each of the 4 drugs, in isolation, in pairs, or in triplet combinations, revealed that the mAbs share functional features that differ from the qualities shared by the two TKIs. For example, unlike the mAbs, osimertinib strongly increased reactive oxygen species (ROS) and the phosphorylated form of histone 2AX (pH2AX). Remarkably, triplets combining osimertinib, an anti-EGFR antibody, and either bemcentinib or mAb654 were initially effective, but longer monitoring in animal models uncovered superiority of the mAb654-containing triplet. In an effort to harness this therapeutic superiority, we designed a bsAb, which co-targeted EGFR and AXL and significantly delayed the onset of resistance to osimertinib when tested *in vivo*.

RESULTS

In vitro effects of singly applied anti-EGFR and anti-AXL drugs

The PC9 lung adenocarcinoma cell line harbors a deletion in exon 19 of the *EGFR* gene. Because this line exhibits high sensitivity to EGFR-specific TKIs, it is widely used by studies interested in mechanisms underlying acquisition of drug resistance.[40] In addition to the clinically approved anti-EGFR drugs, osimertinib and cetuximab, we employed bemcentinib (also called R428 or BGB324), an anti-AXL kinase inhibitor. This drug well discriminates between AXL and the other members of the TAM family (i.e., TYRO3 and MERTK). For comparative analyses, our experiments made use of an anti-AXL antibody, mAb654, which we previously generated and described.[27] Although all four agents inhibited viability of PC9 cells, they clearly fell into 2 groups: unlike the TKIs, especially osimertinib, which killed almost all cells following 72 h of incubation, the effects of the mAbs were weaker (Figures 1A and S1A). These differences were supported by an alternative assay, which utilized crystal violet staining as a measure of cells surviving longer exposure to the drugs (7 days; Figure 1B). Notably, cetuximab was more effective than mAb654 and, correspondingly, osimertinib was more inhibitory than bemcentinib, in line with driver role played by mutant EGFR in PC9 cells, unlike AXL, which plays a compensatory function. As a complementary assay, we probed drug-treated cells for Ki67, a cell proliferation marker that accumulates during the S, G2, and M phases of the cell cycle but undergoes degradation in G1 and G0. The Ki67 results we obtained indicated that all 4 drugs inhibited cell proliferation, but the differences between the effects of mAbs and TKIs were relatively small, likely due to the shorter time of incubation (72 h; Figures 1C and S1B). To better understand the differences between the actions of the two mAbs and two KIs, we performed longer-term assays: a clonogenic assay (14 days; Figures 1D and S1C) and a drug tolerance (persistence) test (9 days; Figures 1E and S1D). Notably, the colony formation assay examines the ability of a single cell to grow into a colony, whereas the persistence assay measures drug tolerance.[25] As expected, osimertinib was the most inhibitory drug in both assays.

To confirm the possibility that the pharmacological effects of the four drugs extend to NSCLC cells other than PC9, we analyzed H1975 cells, which harbor the L858R mutation in exon 21 and the T790M mutation in exon 20. As shown in Figures S2A and S2B, the 4 drugs reduced viability of H1975 cells with IC50 values similar to the parameters determined for PC9 cells. Likewise, proliferation of H1975 cells was better inhibited by the TKIs rather than by the antibodies (Figure S2C). This was reflected also by growing cells in a basement membrane extract (BME) under low-attachment conditions

Statistical significance was assessed and presented in the right hand panel using one-way ANOVA followed by Dunnett's multiple comparisons tests. The experiment was repeated thrice.

(C) PC9 cells were seeded on coverslips and treated for 72 h with CTX (10 μg/mL), mAb654 (10 μg/mL), bemcentinib (100 nM), or osimertinib (10 nM). Cells were fixed in paraformaldehyde and incubated with an anti-Ki67 antibody, followed by a secondary antibody. Images were captured using a confocal microscope. Ki67 staining was quantified and normalized using ImageJ. Values represent mean + SEM of three experiments.

(D) Cells were seeded in 6-well plates (1,000 cells/well) and later treated with CTX (10 μg/mL), mAb654 (10 μg/mL), bemcentinib (100 nM), or osimertinib (10 nM). Media were refreshed once every three days. After 14 days, cells were fixed and stained with crystal violet. The numbers of colonies were determined in triplicates, and the experiment was repeated thrice. Shown are the results of one experiment.

(E) PC9 cells were seeded on 6-well plates at high confluency, and on the next day they were treated with either CTX (20 μg/mL), mAb654 (20 μg/mL), bemcentinib (1,000 nM), or osimertinib (3,000 nM). Media and drugs were refreshed once every three days. After nine days, cells were fixed and stained with crystal violet. Five fields per sample were quantified using ImageJ. Values represent mean +SEM of triplicates from three experiments.

(F) PC9 cells were treated for 48 h with CTX (10 μg/mL), mAb654 (10 μg/mL), Bis1 (20 μg/mL), osimertinib (10 nM), or bemcentinib (100 nM) for the indicated drug combinations. Protein extracts were resolved, blotted, and probed with antibodies specific to the indicated apoptosis, proliferation, and cell-cycle markers. Vinculin and tubulin were used to control gel loading. *, $p < 0.05$; ****, $p < 0.001$.

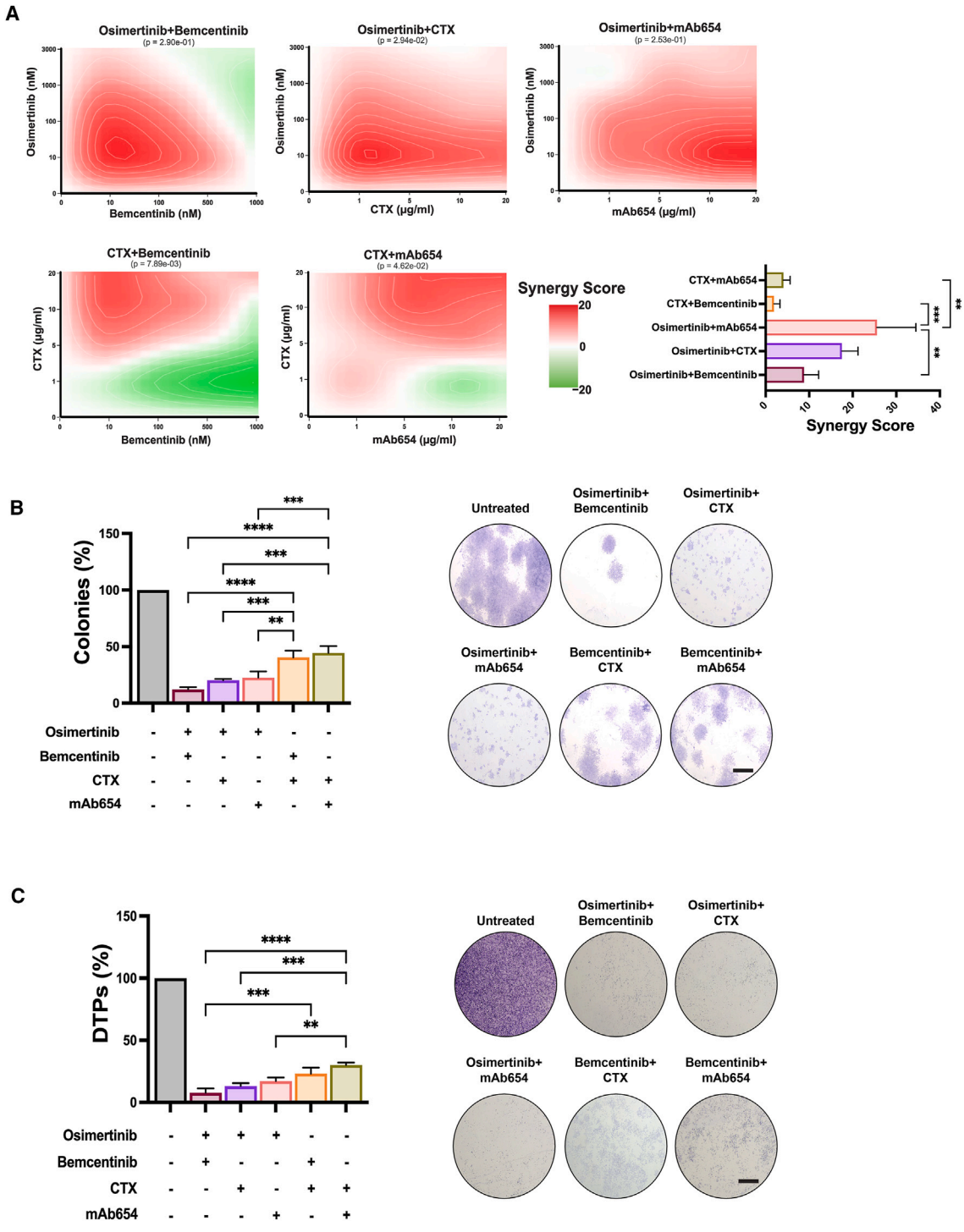

Figure 2. *In vitro* analyses of the biological effects of pairwise combinations of anti-EGFR and anti-AXL drugs

(A) PC9 cells (3×10^3 cells/well) were seeded in 96-well plates and treated for 72 h with increasing concentrations of cetuximab (CTX), mAb654, bemcentinib, and osimertinib, in pairwise combinations. Cell viability was assessed using crystal violet, and the synergy scores were calculated using the Loewe additivity model. Note that the red color marks drug-drug cooperative interactions.

(B) Cells were seeded in 6-well plates (1,000 cells/well) and later treated with dual combinations of CTX (10 μg/mL), mAb654 (10 μg/mL), bemcentinib (100 nM), and osimertinib (10 nM). Media were refreshed once every three days. Following 14 days of incubation, cells were fixed and stained with crystal violet. Shown are bar plots corresponding to one of three experiments (performed in triplicates) and representative photos of individual plates. Bar, micrometers.

(legend continued on next page)

(Figure S2D), a colony formation assay (Figure S2E), and drug tolerance assays (Figure S2F; note that the BME assays did not include bemcentinib and the latter two assays used drug combinations that will be later described). Next, we analyzed extracts isolated from drug-treated H1975 cells. As expected, treatment with osimertinib, more than other treatments, reduced the abundance of cyclin B (Figure 1F), a crucial regulator of the transition from the G2 phase to the M phase of the cell cycle. Likewise, osimertinib induced cleavage of both caspase-3 and PARP1, known markers of cells undergoing apoptosis, as well as enhanced phosphorylation of histone H2AX and increased BIM levels, which can predict clinical benefit from EGFR inhibitors.[41] Importantly, cetuximab partly mimicked the effects of osimertinib on multiple apoptosis/growth arrest markers: caspase-3, PARP1, cyclin B, H2AX, and BIM. But bemcentinib only weakly affected H2AX and BIM, whereas mAb654 was ineffective, in line with the inability of both anti-AXL agents to reduce pEGFR. Taken together, both EGFR inhibitors reduced phospho- and total EGFR and induced markers of growth arrest and apoptosis, but the anti-AXL agents were less effective and, in general, the mAbs emerged as milder inhibitors of viability and proliferation of PC9 and H1975 cells.

Analyses of pairwise and triplet drug combinations unveil cooperative actions of anti-EGFR and anti-AXL drugs

Two models are commonly used to study combined effects of drugs: the Bliss and the Loewe models.[42] Practically, the Bliss model considers the dose-response curves of individual drugs and makes visual representations of each pair of drugs based on data corresponding to multi-dose combination responses. Accordingly, we treated PC9 cells for 72 h with dual combinations of cetuximab (CTX), mAb654, bemcentinib, and osimertinib and assessed viability using crystal violet staining. The results were used for the calculation of drug-drug interactions (synergy scores), as shown in Figure 2A. Note that the combination mAb654+bemcentinib was excluded from the analysis. As expected, due to the relatively high potency of osimertinib, pairs containing osimertinib, especially osimertinib plus an antibody, received high synergy scores. In contrast, due to the lower potency of cetuximab, the respective pairs, including cetuximab+bemcentinib, achieved relatively low synergy scores. Subsequent long-term colony formation assays that were performed with PC9 and H1975 cells (14 days; Figures 2B and S2E) and DTP tests (9 days, Figures 2C and S2F) indicated that all three osimertinib-containing pairs of drugs, especially the combination of the two TKIs, were more inhibitory than the other combinations. Reciprocally, the least inhibitory pair comprised two antibodies (cetuximab+mAb654). To substantiate the relative potency of drug pairs, we probed lysates of H1975 cells and noted that the combination of two TKIs better reduced pAKT and cyclin B, whereas combinations comprising osimertinib and either cetuximab or mAb654 were characterized by moderate or high pH2AX, as well as low EGFR and AXL, respectively (Figure 1F).

Next, we analyzed drug triplets. To this end, an anti-AXL drug, either bemcentinib or mAb654, was separately combined with the pair osimertinib+cetuximab, and the synergy scores of the two triplets were calculated using the additivity model (Figure 3A). While both triplets were clearly cooperative, the combination comprising mAb654, in general, received higher scores than the other triplet (i.e., cetuximab+osimertinib+bemcentinib). Complementary viability, clonogenic, and drug tolerance assays (Figures 3B–3D) confirmed small but consistent superiority of the osimertinib+cetuximab+mAb654 triplet, but cell staining that used an anti-Ki67 antibody failed resolving a difference, although it clearly demonstrated that each triplet achieved better Ki67 inhibition than all drug doublets we examined (Figure 3E). To unveil potential reasons for the superiority of the triplets, we extracted cells following drug treatment and performed immunoblotting (Figure 3F). This confirmed that untreated PC9 cells express active (phosphorylated) forms of EGFR, ERK1/2, and AKT. Importantly, treatment with either triplet reduced EGFR abundance, likely due to cetuximab-mediated receptor endocytosis, and also diminished phosphorylation of EGFR's downstream kinases, AKT and ERK1/2. Concomitantly, the abundance of ERK1/2 and AXL increased and decreased, respectively. Although interesting, these observations fell short of explaining why the two drug triplets acted as superior inhibitors of cell proliferation. Hence, we made use of H1975 cells and extended the analysis to multiple markers of apoptosis and signaling (Figure 1F). The results indicated that the mAb654-containing triplet better sorted AXL for degradation, while the bemcentinib-containing triplet better inhibited AKT phosphorylation, but other apoptosis markers were similarly affected by the two triplets. In conclusion, using an additivity model, we observed cooperative interactions between anti-EGFR and anti-AXL drugs, especially when using triplet drug combinations. These observations are consistent with functional interactions between AXL and EGFR,[8,43,44] and they indicate that both an anti-AXL antibody and an AXL-specific TKI can cooperate *in vitro* with EGFR-targeting drugs.

Whereas the TKIs elevate ROS, the antibodies inhibit downregulation of DNA repair and induce both ADCC and receptor internalization

Since both triplets encompassed osimertinib and cetuximab, it was not surprising that they elevated markers of apoptosis (Figures 4A and 1F), such as cleavage of PARP1, along with upregulation of BIM and downregulation of both cyclin B and BCL2. In comparison to the various doublets, the triplets more strongly induced PARP1 cleavage and elevation of BAX, but the mAb654-containing triplet induced weaker phosphorylation of H2AX, a marker of double-strand breaks (DSBs)[45] in an immunofluorescence assay (Figure 4B; see also stronger inhibitory effects

(C) PC9 cells were seeded on 6-well plates at high confluence. They were later treated for 9 days using the indicated pairs of drugs. The following drugs were used: CTX (20 μg/mL), mAb654 (20 μg/mL), bemcentinib (1,000 nM), and osimertinib (3,000 nM). Media and drugs were refreshed once every three days. After nine days, cells were fixed and stained with crystal violet. Five fields per treatment were quantified for the remaining drug-tolerant cells. Shown are bar graphs and images from one of three experiments. Image quantification used ImageJ. Signals were normalized to the control wells. Values represent the means + SEM of three experiments. Significance was assessed using one-way ANOVA and Dunnett's multiple comparison test. **, $p < 0.01$; ***, $p < 0.005$; ****, $p < 0.001$.

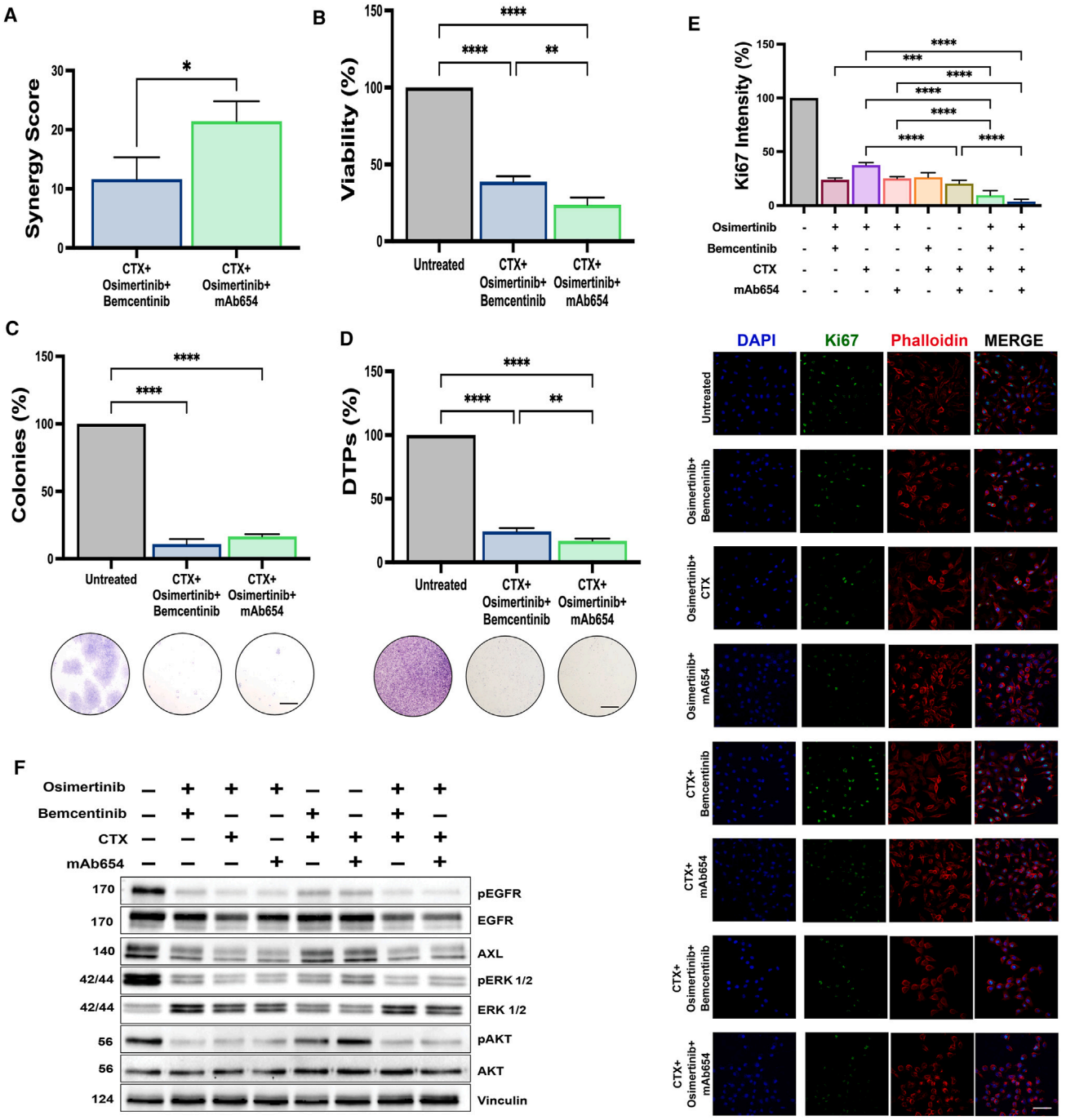

Figure 3. *In vitro* effects of triplet combinations of anti-EGFR and anti-AXL drugs

(A and B) PC9 cells ($3x10^3$ cells/well) were seeded in 96-well plates and treated for 72 h with various concentrations of CTX, mAb654, bemcentinib, or osimertinib. Cell viability was assessed using crystal violet staining, and the synergy score was calculated using the Loewe additivity model.

(C) Cells were seeded in 6-well plates (1,000 cells/well) and later treated with the indicated triple drug combinations. The following drug concentrations were used: CTX (10 μg/mL), mAb654 (10 μg/mL), bemcentinib (100 nM), and osimertinib (10 nM). Media were refreshed once every three days. After 14 days, cells were fixed and stained with crystal violet. Images were captured using an Epson scanner, and colony numbers were determined in triplicates. Bar, 10 μm.

(D) Cells were seeded at high density on 6-well plates. On the next day, cells were treated for nine days with triple drug combinations as follows: CTX (20 μg/mL), mAb654 (20 μg/mL), bemcentinib (1,000 nM), and osimertinib (3,000 nM). Media and drugs were refreshed once every three days. After nine days, the remaining drug-tolerant cells were fixed and stained with crystal violet. Five fields per sample were quantified using ImageJ. Representative microscope fields, along with a bar graph showing normalized signals, are presented. Values represent mean + SEM of three experiments. Bar, 10 μm.

(legend continued on next page)

on DTPs and colony formation by H1975 cells; Figures S2E and S2F). Because ROS are involved in the initial sensing of DSBs, as well as in the later recruitment of H2AX to DSBs,[46] we assayed ROS levels. Although osimertinib elevated ROS production (Figure 4C), we noted that neither cetuximab nor mAb654 affected ROS levels, and bemcentinib only weakly increased ROS. Once again, the mAb654-containing triplet was less effective than the other triplet, implying weaker effects on DNA damage. These observations raised the possibility that antibody-mediated receptor endocytosis and degradation have a role to play in the impact of drug combinations, in line with previously reviewed reports.[47,48] In agreement, immunofluorescence analysis confirmed that EGFR and AXL underwent extensive downregulation and redistribution, consistent with endocytosis, following treatment of PC9 cells with the respective antibody (Figures S3A and S3B). In addition, we confirmed previous reports showing that anti-receptor antibodies can induce extensive antibody-dependent cellular cytotoxicity (ADCC).[49] Of note, our ADCC assay employed cytometry by time of flight (CyTOF) and PC9 cells that were co-cultured with human peripheral blood cells (Figure S3C). Taken together, our observations attributed to both triplets of drugs the ability to induce apoptosis and linked the mAbs to ADCC and receptor internalization, rather than to elevated ROS.

Importantly, TKI-induced ROS are potentially mutagenic. Moreover, according to recent reports, exposure of cancer cells to kinase inhibitors increases their mutation rates by means of simultaneous activation of intrinsic mutators and inhibition of DNA repair.[27,50,51] Hence, we isolated RNA from drug-treated cells and performed PCR analysis using specific primers (see a list of primers in Table S1). The results confirmed that treatment with osimertinib reduced expression of genes involved in homologous recombination (HR) and mismatch repair (MMR) and decreased and enhanced expression of several high-fidelity (proficient) and low-fidelity (mutation-prone) DNA polymerases, respectively (Figure 4D). Notably, treatment with osimertinib elevated AXL and RAD18, the E3 ligase that recruits mutation-prone polymerases to the DNA replication fork.[52,53] In contrast, when mAb654 (or cetuximab) was combined with osimertinib, it inhibited the effects of the latter on the DNA repair enzymes, AXL, RAD18, and mutagenic polymerases. This observation was reflected also in the results obtained with the drug triplets: unlike the triplet osimertinib+cetuximab+bemcentinib, the other combination lost the potentially mutagenic effects on DNA repair and low-fidelity DNA polymerases.

To contrast in an animal model the effects of osimertinib (alone) and the simultaneous mAb-induced inhibition of EGFR and AXL, we made use of an anti-EGFR/AXL bsAb (Bis1) that will be described later. Specifically, PC9 cells were implanted in mice, and after three weeks, when tumors reached approximately 350 mm^3, the animals were randomized into groups that were treated for 7 days, prior to extraction of the regressing tumors and immunoblotting (Figures S3D and S3E). As expected, treatment with osimertinib erased the pEGFR signal but induced less extensive EGFR degradation than Bis1 and cetuximab+osimertinib. Interestingly, the latter group displayed active ERK, but in similarity to other treatments, AXL was downregulated and the effects on DNA polymerases were relatively weak. In terms of proteins involved in the response to DNA damage, all treatments reduced MLH1, RAD18, PCNA, and its ubiquitinated form, but Bis1+osimertinib less extensively downregulated two repair enzymes, MSH2 and RAD51, which respectively ensure the fidelity of DNA replication through MMR and repair of DSBs. Taken together with the results presented in Figure 4, our observations strengthened the conclusion that the modes of action of TKIs and mAbs are fundamentally different: while the TKIs induced ROS and promoted apoptosis, the mAbs we tested inhibited cell proliferation and induced no ROS. Importantly, mAb654 emerged from both dual and triple combinations with osimertinib as an inhibitory drug that can disable the presumably mutagenic actions of osimertinib, namely elevated expression of mutagenic polymerases and reduced expression of DNA repair enzymes. In aggregate, these observations favored the triple drug combination that includes an anti-AXL antibody rather than the AXL-specific TKI.

A drug triplet containing an anti-AXL antibody better delays tumor relapses relative to a triplet containing an AXL-specific kinase inhibitor

We previously reported that, when used alone or in combination with either osimertinib or cetuximab, the anti-AXL antibody could not prevent relapses in the PC9 animal model.[27] Because the previously reported experiments did not include an AXL-specific TKI, we analyzed the effect of bemcentinib on tumor relapses. As expected, neither alone nor in dual combinations (i.e., with osimertinib or cetuximab) was this TKI able to persistently block relapses (Figures 5A–5D) or induce marked adverse effects (Figures S4A and S4B). Next, we examined the prediction that the onset of resistance to a triple drug combination containing an anti-AXL antibody would be delayed relative to a similar combination containing the AXL-specific TKI. To this end, we implanted PC9 cells in mice and, when tumors became palpable, randomized all animals into three groups. One group was left untreated, whereas each of the other groups was treated with a different drug triplet, either cetuximab+osimertinib+mAb654 or cetuximab+osimertinib+bemcentinib. Note that the antibodies were delivered intraperitoneally, twice a week, unlike the TKIs, which were orally delivered once per day.

(E) PC9 cells were seeded on coverslips and treated for 72 h with the indicated double or triple drug combinations. The following drug concentrations were used: CTX (10 μg/mL), mAb654 (10 μg/mL), bemcentinib (100 nM), and osimertinib (10 nM). Cells were fixed in paraformaldehyde and incubated with an anti-Ki67 antibody, followed by a secondary antibody. DAPI was used to stain nuclei. Ki67 staining was quantified and normalized using ImageJ. Values represent mean + SEM of three experiments. Significance was assessed using one-way ANOVA followed by Dunnett's multiple comparison test.

(F) PC9 cells were treated for 48 h with cetuximab (10 μg/mL), mAb654 (10 μg/mL), osimertinib (10 nM), and bemcentinib (100 nM), or with the indicated drug combinations. Cell extracts were resolved, blotted, and probed using antibodies specific to the indicated proteins. Vinculin was used as a gel loading control. *, $p < 0.05$; **, $p < 0.01$; ****, $p < 0.001$.

Please cite this article in press as: Simoni-Nieves et al., A bispecific antibody targeting EGFR and AXL delays resistance to osimertinib, Cell Reports Medicine (2024), https://doi.org/10.1016/j.xcrm.2024.101703

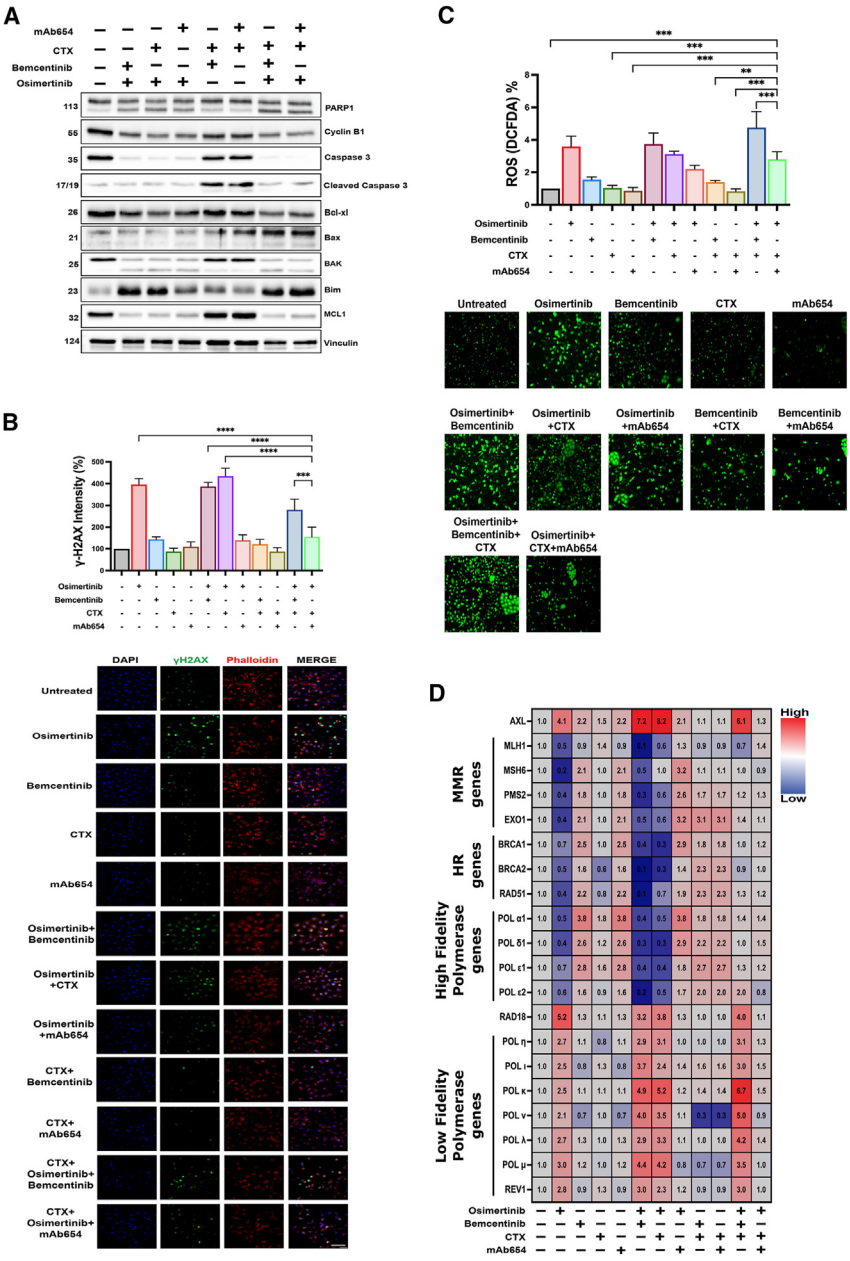

Figure 4. Differential effects of drug combinations on redox potential and enzymes involved in DNA repair and DNA replication

The following drug concentrations were used: CTX and mAb654 (each at 10 μg/mL), bemcentinib (100 nM), and osimertinib (10 nM).

(A) PC9 cells were treated for 48 h with the indicated combinations of cetuximab, mAb654, osimertinib, and bemcentinib. Protein extracts were resolved, blotted, and probed with antibodies specific to the indicated markers.

(B) PC9 cells were seeded on coverslips and treated for 72 h with CTX (10 μg/mL), mAb654 (10 μg/mL), bemcentinib (100 nM), or osimertinib (10 nM), either alone or in combinations. Thereafter, the cells were fixed and incubated with an anti-pH2AX antibody, followed by a secondary antibody (green). DAPI (blue) was used to stain nuclei, and phalloidin (red) was used as a reference. Images were captured using confocal microscopy. Phospho-H2AX staining was quantified and normalized using ImageJ. Representative microscope images are shown. Bar, 20 μm. The Merge column presents an overlay of the other three columns. Significance was assessed using one-way ANOVA and Dunnett's multiple comparison test.

(C) PC9 cells were treated for 6 h using the indicated drugs or their combinations. DCFDA (2',7'-dichlorofluorescin diacetate) was utilized when determining the intracellular content of hydrogen peroxide. Representative images of epifluorescence microscopy are shown (bar, 50 μm), along with quantification of the results (average + SEM). **, $p < 0.01$; ***, $p < 0.005$; ****, $p < 0.001$.

(D) To assay transcription levels corresponding to the indicated genes, we applied quantitative RT-PCR on mRNAs isolated from PC9 cells that underwent pre-treatment for 72 h with the indicated drug combinations. Averages of quadruplicates are shown.

Following 30 days of drug delivery, we stopped all treatments but kept monitoring tumor volumes (Figure 5E), animal survival (Figure 5F), and body weights (Figure S4C). Unlike the control untreated group, all other tumors almost disappeared after two weeks of treatment. However, in line with the *in vitro* data, all mice treated with the combination cetuximab+osimertinib+bemcentinib displayed vigorous, although delayed, relapses soon after treatment cessation. In contrast, no recurrence was observed in the group of animals treated with the other triplet, cetuximab+osimertinib+mAb654. Since the analysis of body weight detected no major changes and the two triplets differed only by the anti-AXL component, we propose the following model: due to the inclusion of osimertinib, cancer cells firstly undergo extensive apoptosis. The few surviving cells activate intrinsic mutators in a mechanism that involves AXL, but nevertheless the newly mutated cells seed relapses in the cetuximab+osimertinib+bemcentinib group. In contrast, because cetuximab and mAb654 reduce mutagenesis, induce receptor endocytosis, and recruit immune effector cells, adaptive mutability and relapses do not occur in the group of animals treated with the other triplet, cetuximab+osimertinib+mAb654.

Construction of a monoclonal anti-EGFR-AXL bsAb

Due to their ability to recognize two different antigens, bsAbs offer pharmacological advantages. We designed an AXL-EGFR bsAb on the basis of two antibodies: the murine form of mAb654 and cetuximab, a human/mouse chimeric molecule. The schematic diagrams shown in Figure 6A depict the recombinant forms of mAb654, cetuximab, and the hybrid, Bis1, which all share a human Fc portion. The amino acid sequence of Bis1 is shown in Table S2. To construct Bis1, we ligated the DNA

Please cite this article in press as: Simoni-Nieves et al., A bispecific antibody targeting EGFR and AXL delays resistance to osimertinib, Cell Reports Medicine (2024), https://doi.org/10.1016/j.xcrm.2024.101703

CellPress
OPEN ACCESS

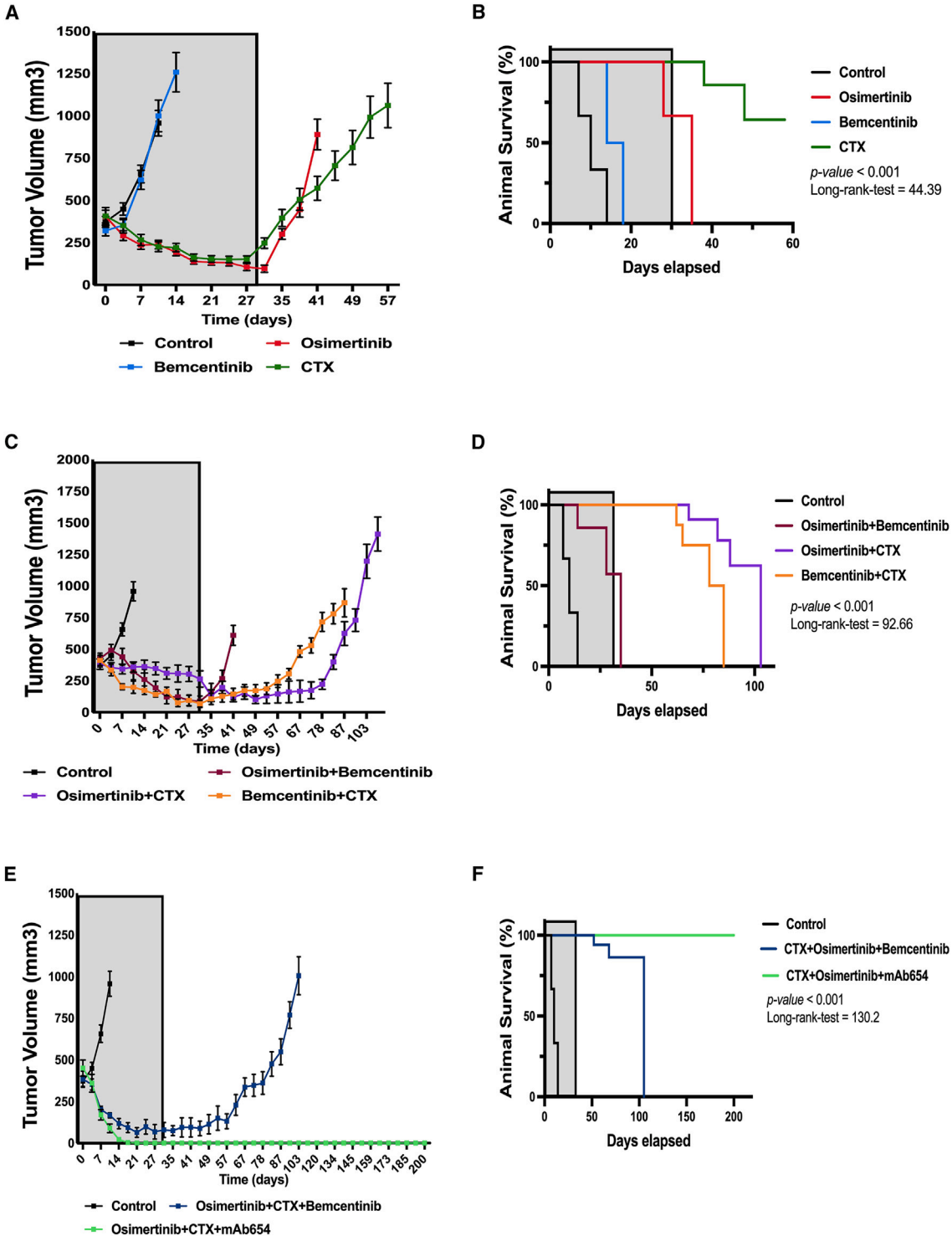

Figure 5. A triplet containing an anti-AXL antibody better inhibits tumor relapses than a triplet containing an anti-AXL kinase inhibitor

PC9 cells (3×10^6 per mouse) were subcutaneously implanted in CD1-nu/nu mice. When tumors reached approximately 350 mm^3, mice were randomized into groups of 5 animals that were treated for 4 weeks (gray area) with either an antibody (CTX or mAb654; 0.2 mg/mouse/injection, once every three days) or TKIs (osimertinibor bemcentinib; 10 and 50 mg/kg/day, respectively, daily). Afterward, we only monitored tumor volumes (left panels) and animal survival (right panels). (A and B) Anti-tumor effects of CTX, osimertinib, and bemcentinib, which were singly delivered. Note that animals were sacrificed once tumors reached 1,500 mm^3.

(legend continued on next page)

Please cite this article in press as: Simoni-Nieves et al., A bispecific antibody targeting EGFR and AXL delays resistance to osimertinib, Cell Reports Medicine (2024), https://doi.org/10.1016/j.xcrm.2024.101703

corresponding to the heavy chain's variable domain of mAb654, as well as the light chain's variable region, into a plasmid encoding human immunoglobulin (Ig)G1. Similarly, we implanted one arm of cetuximab but retained the overall Y-shaped structure. CH1-CL domain swapping ("CrossMab")[54] and CH3 domain knobs-into-holes mutations[55] were introduced into the IgG scaffold to promote the heterodimeric configuration of the bsAb. Bis1 was expressed in human kidney cells and purified in high yields. In addition, Bis1 formed the correct heterodimer combination, with native IgG-like size. Label-free surface plasmon resonance (SPR) measurements were used to determine the binding affinities of the recombinant antibody toward soluble forms of AXL and EGFR, which were immobilized on a sensor chip. The obtained sensograms (Figure S5A) were used to calculate the respective binding affinities. A summary of these parameters is shown in Figure 6B. As indicated, the binding affinity of the recombinant form of mAb654 was 3-fold lower than the parental murine antibody, whereas the affinity of the recombinant form of cetuximab was largely retained. Similar analysis of Bis1 confirmed dual antigen specificities but indicated reduced antigen binding affinity of both arms, probably due to monovalent antigen binding and consequent enhanced dissociation.

Next, we performed an ELISA-based assay that confirmed simultaneous antigen engagement by each arm of Bis1 (Figure S5B). In addition, we performed an immunoprecipitation assay that used PC9 cell extracts and confirmed that Bis1 pulled down both AXL and EGFR (Figure S5C). These tests validated that each arm of Bis1 can simultaneously engage a distinct receptor. To verify that these attributes reconstituted the biological activities of the parental antibodies, as well as the cooperation with osimertinib, we performed the following set of *in vitro* assays, which employed PC9 or H1975 cells: (1) cell viability (Figures 6C and S5D), (2) cell proliferation (Figure 6D), (3) 3D spheroid formation (Figures 6E and S2D), (4) colony formation (Figures 6F, S2E, and S5E), (5) drug tolerance persister test (Figures 6G, S2F, and S5F), (6) Ki67 staining (Figures 6H and S5G), (7) receptor endocytosis tests (Figures S3A and S3B), (8) the lentiviral FUCCI (fluorescent ubiquitination-based cell cycle indicator) cell-cycle assay,[56] which confirmed G1 growth arrest (Figure S5H), and (9) immunoblotting analyses of apoptosis and other markers (Figure 1F). Collectively, the results we obtained indicated that the combination of Bis1 and osimertinib was functionally equivalent to the triplet cetuximab+mAb654+osimertinib.

When combined with osimertinib, a monoclonal EGFR-AXL bsAb inhibits relapses of regular and patient-derived xenograft models

To test the ability of Bis1 to delay emergence of resistance to osimertinib, we performed an *in vivo* study that made use of PC9 cells and athymic mice. As in Figure 5, when tumors became palpable, mice were randomized into groups. Each group of 5–9 animals was daily treated, for 4 weeks, with osimertinib. Alternatively, animals were treated with combinations of osimertinib (daily oral treatments) and mAbs (intraperitoneal delivery, twice per week). To match the recombinant bsAb, we employed recombinant forms of both cetuximab (rCTX) and the anti-AXL antibody (rmAb654). Following termination of all treatments, we kept monitoring tumor volumes (Figures 7A–7F) and body weight (Figure S6A) for up to 6 additional months. Note that animal survival curves corresponding to each experimental arm are presented in Figure 7G.

As opposed to untreated animals (Figure 7A), the tumors of all mice treated with osimertinib alone rapidly shrunk, but they relapsed shortly after the oral treatments were stopped (Figure 7B). Significantly delayed relapses were observed in the group treated with a combination of osimertinib and the recombinant form of cetuximab (Figure 7C). Furthermore, in this group, 3 of the 9 animals (33%) showed no relapses by the end of the experiment. However, a similar combination comprising osimertinib and the recombinant form of mAb654 was less effective (Figure 7D). As expected, the triplet osimertinib+rCTX+rmAb654 delayed the onset of relapses for longer time, and, furthermore, 50% of mice in this group showed no relapses by the time we closed the experiment (Figure 7E). In comparison, Bis1 showed even better results: combining this EGFR-AXL bsAb with osimertinib fully prevented relapses of six of the seven animals of this arm (86%), although mice were treated for only four weeks and they were terminated as long as half a year later (Figure 7F). In summary, the *in vivo* inhibitory action of the EGFR-AXL bsAb we constructed was as strong as or better than the efficacy achieved by the corresponding triple drug combination.

In the next step, we analyzed patient-derived xenografts (PDXs), which better represent intra-tumor heterogeneity than cell line xenografts. An especially aggressive model, TM00193, which expresses E746_A750 Del19-EGFR, was selected for *in vivo* tests. Fragments of the PDX were engrafted, and, when tumors reached approximately 350 mm^3, mice were randomized into groups of 5–9 animals that were treated for 35 days with osimertinib, osimertinib+cetuximab+mAb654, or osimertinib+Bis1. Afterward, we only monitored tumor volumes and recorded animal survival. Note that we employed NSG mice, which have no active T cells, B cells, natural killer (NK) cells, and dendritic cells and applied drug holiday in order to detect early relapses. The resulting average tumor growth curves are presented in Figure 7H, and analyses depicting animal survival and body weight are shown in Figures 7I and S6B, respectively. In agreement with the observations made *in vitro* and with PC9 xenografts, both combination treatments significantly delayed the onset of relapses and extended animal survival, and this exceeded the effect achieved by osimertinib monotherapy. Importantly, the growth curves corresponding to osimertinib+Bis1 and the triplet combination (osimertinib+cetuximab+mAb654) were practically indistinguishable, implying that Bis1 accurately incorporated the functional attributes of its parental antibodies. Presumably, longer treatments (>60 days) and complete tumor eradication while on treatment (prior to the drug holiday) might permit further delay of the onset of drug resistance in this model.

(C and D) Anti-tumor effects of the following drug doublets: CTX combined with either osimertinib or bemcentinib and the combination of the two TKIs.
(E and F) Anti-tumor effects of the following drug triplets: CTX+osimertinib+anti-AXL mAb654 or CTX+osimertinib+bemcentinib. Data shown are means (from 5 animals) ± SEM. Note that, once an animal dies in the course of experimentation, it is eliminated from the calculation of the average tumor volume.

Please cite this article in press as: Simoni-Nieves et al., A bispecific antibody targeting EGFR and AXL delays resistance to osimertinib, Cell Reports Medicine (2024), https://doi.org/10.1016/j.xcrm.2024.101703

CellPress
OPEN ACCESS

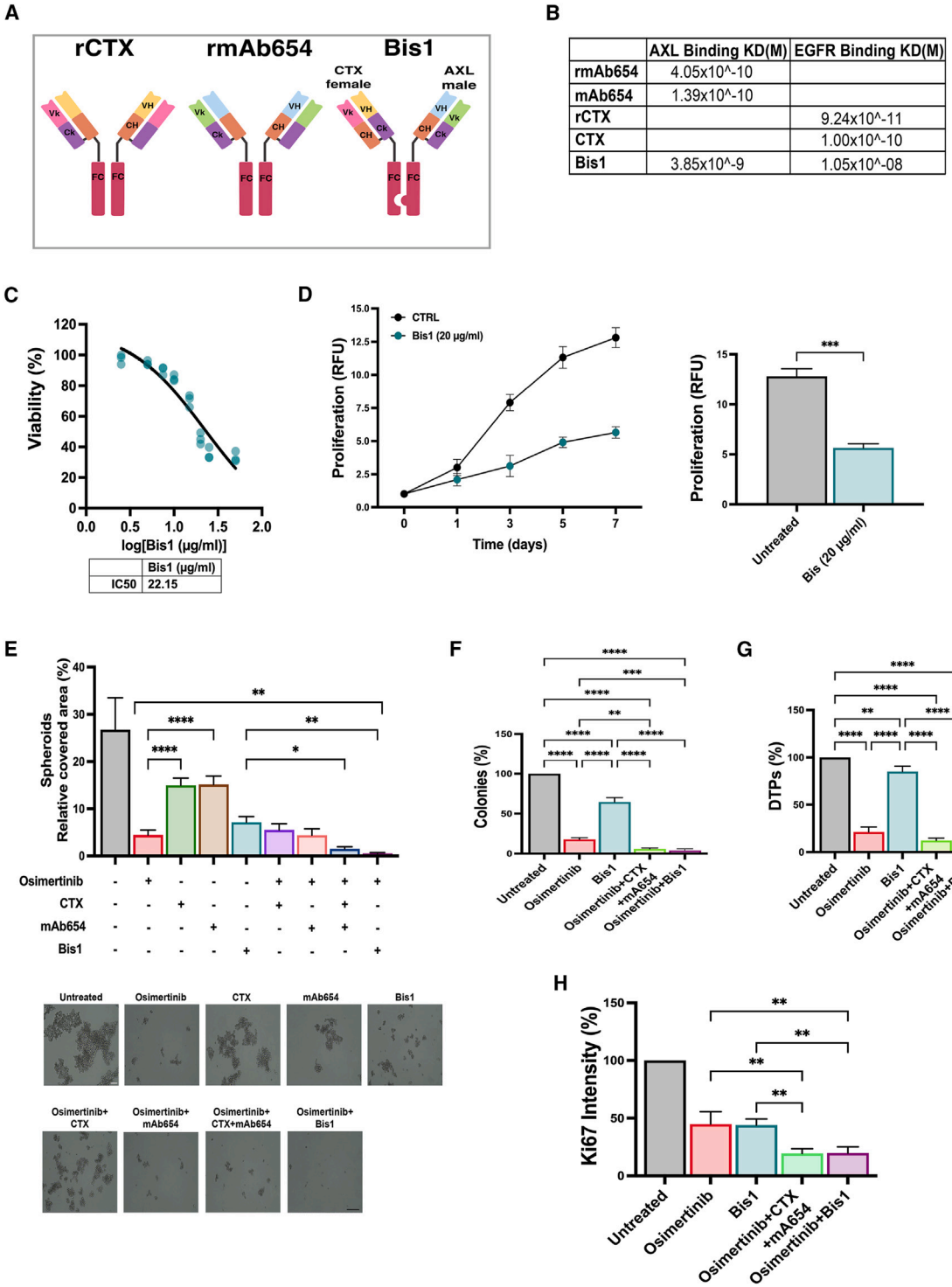

	AXL Binding KD(M)	EGFR Binding KD(M)
rmAb654	4.05x10^-10	
mAb654	1.39x10^-10	
rCTX		9.24x10^-11
CTX		1.00x10^-10
Bis1	3.85x10^-9	1.05x10^-08

	Bis1 (µg/ml)
IC50	22.15

Figure 6. A recombinant bispecific antibody embodies the functional attributes of anti-EGFR and anti-AXL monoclonal antibodies

(A) Schematic representation of the bispecific antibody, Bis1, and both the parental recombinant anti-AXL mAb654 and the recombinant form of mAb654. The human Fc domain of Bis1 (in red) contains a knobs-in-holes configuration. V denotes a variable domain, and C marks a constant antibody domain. Likewise, H denotes a heavy chain and k marks the kappa light chain. CTX, cetuximab.

(B) Surface plasmon resonance (SPR) was used to determine binding affinities of the indicated antibodies, including rmAb654, a recombinant anti-AXL mAb and a recombinant cetuximab (rCTX), to immobilize human AXL and human EGFR. The calculated parameters are indicated.

(C) A viability assay was performed with PC9 cells and Bis1, essentially as described in Figure 1A.

(legend continued on next page)

Please cite this article in press as: Simoni-Nieves et al., A bispecific antibody targeting EGFR and AXL delays resistance to osimertinib, Cell Reports Medicine (2024), https://doi.org/10.1016/j.xcrm.2024.101703

In summary, by contrasting a mAb and a kinase inhibitor, both targeting the same compensatory receptor, AXL, we aimed at resolving mechanisms of resistance to osimertinib, as well as prolonging the efficacy of this TKI. Our initial experiments indicated that no dual combination of osimertinib and an anti-AXL drug was as effective as triple combinations that included an AXL inhibitor, either a TKI or an mAb, in combination with osimertinib and an anti-EGFR antibody (cetuximab). Unlike the mAbs, osimertinib robustly elevated ROS and downregulated DNA repair enzymes. In line with distinct mechanisms of drug action, xenografts treated with the triplet containing the AXL-specific TKI eventually relapsed, but nearly all animals treated with the triplet containing an anti-AXL antibody remained tumor free in a cell line xenograft model. To reduce the pharmacological complexity of the more consistent triplet, we designed a monoclonal EGFR-AXL bsAb, which persistently delayed relapses, not only in a cell line xenograft system but also in a patient-derived model. These observations are discussed in the following in terms of mechanisms driving drug action, resistance to osimertinib, and the prospects for clinical application.

DISCUSSION

Our study questions the current practice of treating patients with EGFR-mutated lung cancer. Despite initial response to the first-generation EGFR-specific TKIs, nearly all patients acquire drug resistance, and the most common mechanism of resistance involves a secondary EGFR mutation (T790M).[7] Although the third-generation irreversible inhibitor, osimertinib, can inhibit T790M-EGFR and it has been approved as second-[13] and first-line therapy,[14] emergence of a secondary mutation, C797S, once again underlays acquired resistance, albeit in a smaller fraction of patients.[15] Notably, recurring resistance-conferring mutations are similarly manifested by acute myeloid leukemia treated with BCR-ABL inhibitors[57] and TKI-treated ALK-positive lung cancer.[58] In contrast, anti-cancer treatments making use of antibodies seldom evoke secondary mutations.[59,60] Because many mAbs, unlike many TKIs, do not kill cancer cells, they are often combined with cytotoxic treatments, such as chemotherapy or radiotherapy, but combinations with TKIs are not common.[61] These distinct pharmacological attributes of mAbs are relevant to EGFR-mutated lung cancer because overexpression of *AXL*[8] and amplification of *MET*[62] or *HER2*[9] drive resistance to first-generation TKIs and might precede emergence of the T790M mutation. Likewise, *MET* or *HER2* amplification, along with C797S, are the most common mechanisms of resistance to osimertinib in first-line settings.[15] Based on the accessibility of MET, HER2, and AXL to therapeutic antibodies, as well as the reported roles for AXL in the emergence of additional EGFR mutations,[8,27] our study explored various combinations of AXL- and EGFR-specific mAbs and TKIs. Comparative analysis of single drugs, along with their dual and triple combinations, made it clear that triplets were more effective blockers of indicator cell lines and targeting EGFR, the driver, was more effective than targeting AXL. These observations led us to contrast two triplets and eventually select a combination that included an anti-AXL mAb (in addition to osimertinib and cetuximab) rather than an anti-AXL-specific TKI. Eventually, we combined the pharmacological attributes of the two antibodies by designing a bispecific EGFR-AXL antibody, which holds therapeutic promise.

Why would a triplet comprising an anti-AXL mAb surpass *in vivo* a triplet that includes an anti-AXL TKI? According to our results, the latter treatment, which contains osimertinib, bemcentinib, and cetuximab, more strongly induces ROS and cell death relative to the triplet containing two mAbs. In addition, our data and previous reports[27,51] propose that the keys to the greater therapeutic activity of the two-mAb triplet might be the ability of the anti-AXL antibody to enhance receptor internalization and ADCC, as well as inhibit treatment-induced mutagenesis. The adaptive mutability response is multifaceted: in response to drug-induced cell death, AXL undergoes upregulation and stimulates the SOS response, which engages several intrinsic mutators, as well as downregulates the DNA damage response.[27,51] Specifically, following treatment with a TKI, such as osimertinib, both MMR and HR repair genes undergo downregulation, as do several high-fidelity DNA polymerases. Thus, through blocking the very initial step of this cascade, namely binding of AXL to GAS6 at the surface of dying cells, the anti-AXL antibody might inhibit mutagenesis but still permit TKI-induced death of cancer cells.

Unlike bemcentinib, anti-AXL mAb654 can potentially recruit immune effector cells, which might explain the long-term efficacy of the mAb654-containing triplet, as well as the potency of Bis1. Although our animal model lacks T lymphocytes, NK, other cells, and the Fc portion of mAb654 might be involved in heightening the response to mAb654. In line with this scenario, it was shown that tumor regression elicited by osimertinib involves local accumulation of tumor-associated macrophages.[63] Alternatively, anti-AXL antibodies, in similarity to cetuximab, might harness non-immune mechanisms, such as antibody-induced clearance of AXL from the cell surface via a universal

(D) Shown are the results of a PC9 cell proliferation assay that was performed in triplicates with Bis1 (20 μg/mL), as detailed in the legend to Figure 1B.
(E) PC9 cells were cultured under low-attachment conditions, leading to the formation of 3D spheroids. A total of 500 cells were plated in 6-well plates, which were pre-coated with agar (0.6%), in a complete medium containing the indicated treatments, including Bis1 (10 μg/mL). After 7 days, multiple images from non-overlapping fields were captured. Scale bar, 100 μm. The percentage of covered area was calculated. The results are represented as the average of two independent experiments. *, $p < 0.05$; **, $p < 0.01$; ***$p < 0.001$.
(F) PC9 cells were treated with CTX (10 μg/mL), mAb654 (10 μg/mL), Bis1 (10 μg/mL), or osimertinib (10 nM). After 14 days, cells were fixed and stained with crystal violet and the numbers of colonies were determined in triplicate as described in the legend to Figure 1D.
(G) PC9 cells were seeded in 6-well plates at high confluency, and on the next day they were treated as in (F). Media and drugs were refreshed once every three days. After 9 days, cells were fixed and stained with crystal violet. Five fields per sample were quantified using ImageJ. Signals were normalized to the control wells. Values represent mean + SEM of triplicates from three experiments.
(H) PC9 cells were seeded on coverslips and treated for 72 h as in (F). Cells were fixed and probed using an anti-Ki67 antibody, followed by a secondary antibody. Ki67 staining was quantified and normalized using ImageJ. *, $p < 0.05$; **, $p < 0.01$; ***, $p < 0.005$; ****, $p < 0.001$.

Please cite this article in press as: Simoni-Nieves et al., A bispecific antibody targeting EGFR and AXL delays resistance to osimertinib, Cell Reports Medicine (2024), https://doi.org/10.1016/j.xcrm.2024.101703

CellPress
OPEN ACCESS

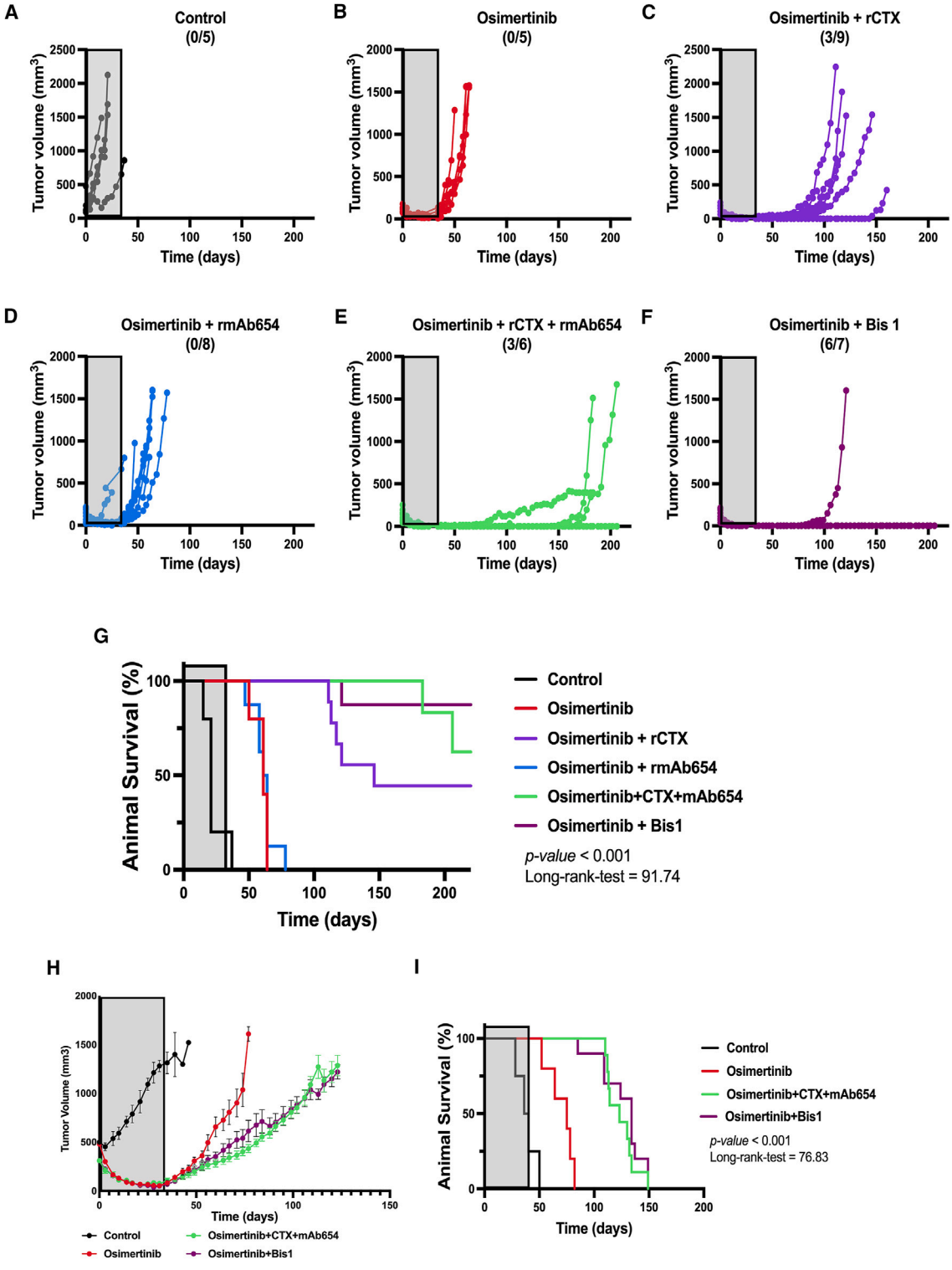

Figure 7. The monoclonal EGFR-AXL bispecific antibody, Bis1, inhibits relapses of regular and patient-derived xenograft models when combined with osimertinib

(A–F) PC9 cells were subcutaneously implanted in the flanks of CD1-nu/nu mice. When tumors became palpable, mice were randomized in groups of 5–7 animals that were treated (gray areas) for 30 days with the indicated antibodies (0.2 mg/mouse/injection) once every three days, or daily with osimertinib (10 mg/kg/day). Shown are tumor volumes corresponding to individual mice. The number of mice free of relapses is indicated per each group.

(G) Shown are survival curves corresponding to (A–F), along with statistical parameters. Note that mice were sacrificed once tumor volume exceeded 1,500 mm^3.

(legend continued on next page)

clathrin-mediated endocytosis that involves dynamin 2.[64] In this context, it is worth noting that proteolysis targeting chimeras (PROTACs) aiming at EGFR have been developed,[65] including a compound that sorted mutant EGFRs for degradation.[66] This raises the possibility that AXL-targeting PROTACs, in combination with osimertinib and cetuximab, might delay tumor relapses. Our study raises additional therapeutic predictions, beyond demonstrating *in vivo* activity of the bsAb we constructed. Blocking GAS6, a ligand of both AXL and phosphatidylserine, which externalizes on apoptotic cells, might reduce the ability of AXL to sense stress and trigger endogenous mutators. Likewise, pharmacologically targeting the mutagenic DNA polymerases recruited to sites of DNA damage, as well as their coordinator, RAD18,[67] might delay relapses. Furthermore, the concerted upregulation of mutagenic DNA polymerases and downregulation of DNA repair enzymes might herald tumor relapse and hence identify early biomarkers of AXL-mediated resistance to osimertinib. Confirming the prognostic value of mutagenic enzymes, as well as the therapeutic benefit from the herein described EGFR-AXL bsAb, will necessitate further tests in animals and might lead to clinical trials.

Limitations of the study

Although our results clearly attribute superior resitance-delaying effects to a drug combination that includes an anti-AXL antibody, rather than an anti-AXL kinase inhibitor, and we attributed the underlying mechanism to redox and DNA repair, the exact details remain unresolved. In addition, even though our study employed two widely used models of EGFR-mutated cancer cells, PC9 and H1975, which harbor the most prevalent EGFR mutation types, testing additional cellular and animal models might be important. For example, effective treatment of tumors harboring the highly prevalent mutation, L858R, can be achieved by a single antibody, cetuximab, with no need to include additional antibodies or a kinase inhibitor.[68] Hence, extending the analyses we performed to other mutant forms of EGFR, as well as to other strains of mice, would be needed prior to attempts to establish clinical relevance. For instance, our study utilized immunocompromised mice, but we cannot exclude the possibility that T and B lymphocytes, which are not present in the recipient animals employed by our experiments, play major roles in resistance to EGFR-specific kinase inhibitors. Likewise, our study underscored the critical roles played by compensatory signaling pathways, such as the AXL's pathway. However, we have not addressed the roles played by AXL's ligand, GAS6, and specific mutagenic enzymes, such as APOBEC and the mutational signatures that might characterize their action at the genome level.[50,69] Furthermore, we constructed only one bsAb, although constructing additional bsAbs, which have smaller size or a toxic payload, is expected to increase the translational dimension of our work. Along these lines, the uncovered superiority of a mAb relative to TKI might extend to MERTK and HER2, the closest paralogs of AXL and EGFR, respectively, and thereby motivate clinical development of additional bispecific antibodies.

RESOURCE AVAILABILITY

Lead contact

Further information and requests for resources and reagents should be directed to and will be fulfilled by the lead contact, Prof. Yosef Yarden (yosef.yarden@weizmann.ac.il).

Materials availability

This study generated a bispecific antibody that will be made available upon request.

Data and code availability

- All data reported in this article will be shared by the lead contact upon request.
- This paper does not report original codes.
- Any additional information required to re-analyze the data reported in this paper is available from the lead contact upon request.

ACKNOWLEDGMENTS

We thank all members of our laboratories for their kind help and insightful comments. This work was performed in the Marvin Tanner Laboratory for Research on Cancer. Y.Y. is the incumbent of the Harold and Zelda Goldenberg Professorial Chair in Molecular Cell Biology. Our studies were supported by Merck KGaA, the Israel Science Foundation, the European Research Council (ERC), the Israel Cancer Research Fund (ICRF), and the Dr. Miriam and Sheldon G. Adelson Medical Research Foundation.

AUTHOR CONTRIBUTIONS

Conceptualization, A.S.-N., M. Lindzen, I.M., and Y.Y.; methodology, A.S.-N., M. Lindzen, D.R., M. Lauriola, N.G., R.C., M.V.D., D.L., and S.G.; formal analysis, A.S.-N., M. Lindzen, S.G., T.-M.S., and B.R.-S.; investigation, A.S.-N., M. Lindzen, Y.H., Y.T., and S.G.; resources, M. Lindzen, N.G., R.C., R.O., M.Z., and S.G.; writing – original draft, I.M. and Y.Y.; writing – review, all authors; supervision, M. Lindzen and Y.Y.; project administration, A.S.-N., M. Lindzen, and Y.Y.; funding acquisition, Y.Y.

DECLARATION OF INTERESTS

We, the authors, plan to file a patent application for the bispecific antibody (EGFR/AXL), namely Bis1, which has been developed in this study.

STAR★METHODS

Detailed methods are provided in the online version of this paper and include the following:

- KEY RESOURCES TABLE
- EXPERIMENTAL MODEL AND STUDY PARTICIPANT DETAILS
  - Cell cultures
  - Animal studies
- METHOD DETAILS
  - Cell viability assays
  - Cell proliferation assays

(H) Fragments of the PDXJ3 patient-derived xenograft (E746_A750 Del19-EGFR) were engrafted in NSG mice. When tumors reached approximately 350 mm^3, mice were randomized into groups of 5–9 animals that were intraperitoneally treated (gray areas) for 30 days with the indicated antibodies (CTX or mAb654; 0.1 mg/mouse/injection, and Bis1; 0.2 mg/mouse/kg, once every three days) and/or oral osimertinib (5 mg/kg/day). Afterward, we only monitored tumor volumes and recorded the average tumor volumes. Data shown are means (from 5 to 9 animals) ± SEM.
(I) Shown are survival curves and statistical parameters corresponding to the four groups of mice shown in (H).

- Immunofluorescence analysis
- Colony formation assays
- Immunoblotting and ELISA assays
- ROS production assays
- RNA isolation and real-time PCR
- Surface plasmon resonance (SPR) measurements
- Drug synergy analysis
- Design and expression of recombinant antibodies
- Cell cycle distribution using Fucci
- Spheroid assays
- ADCC assays

- QUANTIFICATION AND STATISTICAL ANALYSIS

SUPPLEMENTAL INFORMATION

Supplemental information can be found online at https://doi.org/10.1016/j.xcrm.2024.101703.

Received: December 18, 2023
Revised: June 19, 2024
Accepted: August 7, 2024
Published: August 30, 2024

REFERENCES

1. Cancer Genome Atlas Research Network (2014). Comprehensive molecular profiling of lung adenocarcinoma. Nature *511*, 543–550. https://doi.org/10.1038/nature13385.
2. Negrao, M.V., Skoulidis, F., Montesion, M., Schulze, K., Bara, I., Shen, V., Xu, H., Hu, S., Sui, D., Elamin, Y.Y., et al. (2021). Oncogene-specific differences in tumor mutational burden, PD-L1 expression, and outcomes from immunotherapy in non-small cell lung cancer. J. Immunother. Cancer *9*, e002891. https://doi.org/10.1136/jitc-2021-002891.
3. Jiao, X.D., He, X., Qin, B.D., Liu, K., Wu, Y., Liu, J., Hou, T., and Zang, Y.S. (2019). The prognostic value of tumor mutation burden in EGFR-mutant advanced lung adenocarcinoma, an analysis based on cBioPortal data base. J. Thorac. Dis. *11*, 4507–4515. https://doi.org/10.21037/jtd.2019.11.04.
4. Mitsudomi, T., Morita, S., Yatabe, Y., Negoro, S., Okamoto, I., Tsurutani, J., Seto, T., Satouchi, M., Tada, H., Hirashima, T., et al. (2010). Gefitinib versus cisplatin plus docetaxel in patients with non-small-cell lung cancer harbouring mutations of the epidermal growth factor receptor (WJTOG3405): an open label, randomised phase 3 trial. Lancet Oncol. *11*, 121–128. https://doi.org/10.1016/S1470-2045(09)70364-X.
5. Rosell, R., Carcereny, E., Gervais, R., Vergnenegre, A., Massuti, B., Felip, E., Palmero, R., Garcia-Gomez, R., Pallares, C., Sanchez, J.M., et al. (2012). Erlotinib versus standard chemotherapy as first-line treatment for European patients with advanced EGFR mutation-positive non-small-cell lung cancer (EURTAC): a multicentre, open-label, randomised phase 3 trial. Lancet Oncol. *13*, 239–246. https://doi.org/10.1016/s1470-2045(11)70393-x.
6. Zhou, C., Wu, Y.L., Chen, G., Feng, J., Liu, X.Q., Wang, C., Zhang, S., Wang, J., Zhou, S., Ren, S., et al. (2011). Erlotinib versus chemotherapy as first-line treatment for patients with advanced EGFR mutation-positive non-small-cell lung cancer (OPTIMAL, CTONG-0802): a multicentre, open-label, randomised, phase 3 study. Lancet Oncol. *12*, 735–742. https://doi.org/10.1016/S1470-2045(11)70184-X.
7. Pao, W., Miller, V.A., Politi, K.A., Riely, G.J., Somwar, R., Zakowski, M.F., Kris, M.G., and Varmus, H. (2005). Acquired resistance of lung adenocarcinomas to gefitinib or erlotinib is associated with a second mutation in the EGFR kinase domain. PLoS Med. *2*, e73.
8. Zhang, Z., Lee, J.C., Lin, L., Olivas, V., Au, V., LaFramboise, T., Abdel-Rahman, M., Wang, X., Levine, A.D., Rho, J.K., et al. (2012). Activation of the AXL kinase causes resistance to EGFR-targeted therapy in lung cancer. Nat. Genet. *44*, 852–860. https://doi.org/10.1038/ng.2330.
9. Takezawa, K., Pirazzoli, V., Arcila, M.E., Nebhan, C.A., Song, X., de Stanchina, E., Ohashi, K., Janjigian, Y.Y., Spitzler, P.J., Melnick, M.A., et al. (2012). HER2 amplification: a potential mechanism of acquired resistance to EGFR inhibition in EGFR-mutant lung cancers that lack the second-site EGFRT790M mutation. Cancer Discov. *2*, 922–933. https://doi.org/10.1158/2159-8290.Cd-12-0108.
10. Schwarz, L.J., Hutchinson, K.E., Rexer, B.N., Estrada, M.V., Gonzalez Ericsson, P.I., Sanders, M.E., Dugger, T.C., Formisano, L., Guerrero-Zotano, A., Red-Brewer, M., et al. (2017). An ERBB1-3 Neutralizing Antibody Mixture With High Activity Against Drug-Resistant HER2+ Breast Cancers With ERBB Ligand Overexpression. J. Natl. Cancer Inst. *109*, djx065. https://doi.org/10.1093/jnci/djx065.
11. Mueller, K.L., Madden, J.M., Zoratti, G.L., Kuperwasser, C., List, K., and Boerner, J.L. (2012). Fibroblast-secreted hepatocyte growth factor mediates epidermal growth factor receptor tyrosine kinase inhibitor resistance in triple-negative breast cancers through paracrine activation of Met. Breast Cancer Res. *14*, R104. https://doi.org/10.1186/bcr3224.
12. Yano, S., Wang, W., Li, Q., Matsumoto, K., Sakurama, H., Nakamura, T., Ogino, H., Kakiuchi, S., Hanibuchi, M., Nishioka, Y., et al. (2008). Hepatocyte growth factor induces gefitinib resistance of lung adenocarcinoma with epidermal growth factor receptor-activating mutations. Cancer Res. *68*, 9479–9487. https://doi.org/10.1158/0008-5472.Can-08-1643.
13. Mok, T.S., Wu, Y.-L., Ahn, M.-J., Garassino, M.C., Kim, H.R., Ramalingam, S.S., Shepherd, F.A., He, Y., Akamatsu, H., Theelen, W.S.M.E., et al. (2017). Osimertinib or Platinum-Pemetrexed in EGFR T790M-Positive Lung Cancer. N. Engl. J. Med. *376*, 629–640.
14. Soria, J.-C., Ohe, Y., Vansteenkiste, J., Reungwetwattana, T., Chewaskulyong, B., Lee, K.H., Dechaphunkul, A., Imamura, F., Nogami, N., Kurata, T., et al. (2018). Osimertinib in Untreated EGFR-Mutated Advanced Non-Small-Cell Lung Cancer. N. Engl. J. Med. *378*, 113–125.
15. Ramalingam, S.S., Yang, J.C.H., Lee, C.K., Kurata, T., Kim, D.W., John, T., Nogami, N., Ohe, Y., Mann, H., Rukazenkov, Y., et al. (2018). Osimertinib As First-Line Treatment of EGFR Mutation-Positive Advanced Non-Small-Cell Lung Cancer. J. Clin. Oncol. *36*, 841–849. https://doi.org/10.1200/JCO.2017.74.7576.
16. Chmielecki, J., Gray, J.E., Cheng, Y., Ohe, Y., Imamura, F., Cho, B.C., Lin, M.C., Majem, M., Shah, R., Rukazenkov, Y., et al. (2023). Candidate mechanisms of acquired resistance to first-line osimertinib in EGFR-mutated advanced non-small cell lung cancer. Nat. Commun. *14*, 1070. https://doi.org/10.1038/s41467-023-35961-y.
17. Chmielecki, J., Mok, T., Wu, Y.L., Han, J.Y., Ahn, M.J., Ramalingam, S.S., John, T., Okamoto, I., Yang, J.C.H., Shepherd, F.A., et al. (2023). Analysis of acquired resistance mechanisms to osimertinib in patients with EGFR-mutated advanced non-small cell lung cancer from the AURA3 trial. Nat. Commun. *14*, 1071. https://doi.org/10.1038/s41467-023-35962-x.
18. Gazdar, A.F. (2009). Activating and resistance mutations of EGFR in non-small-cell lung cancer: role in clinical response to EGFR tyrosine kinase inhibitors. Oncogene *28*, S24–S31. https://doi.org/10.1038/onc.2009.198.
19. Vyse, S., and Huang, P.H. (2019). Targeting EGFR exon 20 insertion mutations in non-small cell lung cancer. Signal Transduct. Target. Ther. *4*, 5. https://doi.org/10.1038/s41392-019-0038-9.
20. Sequist, L.V., Waltman, B.A., Dias-Santagata, D., Digumarthy, S., Turke, A.B., Fidias, P., Bergethon, K., Shaw, A.T., Gettinger, S., Cosper, A.K., et al. (2011). Genotypic and histological evolution of lung cancers acquiring resistance to EGFR inhibitors. Sci. Transl. Med. *3*, 75ra26.
21. Niederst, M.J., Hu, H., Mulvey, H.E., Lockerman, E.L., Garcia, A.R., Piotrowska, Z., Sequist, L.V., and Engelman, J.A. (2015). The allelic context of the C797S mutation acquired upon treatment with third generation EGFR inhibitors impacts sensitivity to subsequent treatment strategies. Clin. Cancer Res. *21*, 3924–3933. https://doi.org/10.1158/1078-0432.CCR-15-0560.
22. Thress, K.S., Paweletz, C.P., Felip, E., Cho, B.C., Stetson, D., Dougherty, B., Lai, Z., Markovets, A., Vivancos, A., Kuang, Y., et al. (2015). Acquired EGFR C797S mutation mediates resistance to AZD9291 in non-small

cell lung cancer harboring EGFR T790M. Nat. Med. *21*, 560–562. https://doi.org/10.1038/nm.3854.

23. Hill, W., Lim, E.L., Weeden, C.E., Lee, C., Augustine, M., Chen, K., Kuan, F.C., Marongiu, F., Evans, E.J., Jr., Moore, D.A., et al. (2023). Lung adenocarcinoma promotion by air pollutants. Nature *616*, 159–167. https://doi.org/10.1038/s41586-023-05874-3.
24. Radman, M. (1975). SOS repair hypothesis: phenomenology of an inducible DNA repair which is accompanied by mutagenesis. Basic Life Sci. *5A*, 355–367. https://doi.org/10.1007/978-1-4684-2895-7_48.
25. Sharma, S.V., Lee, D.Y., Li, B., Quinlan, M.P., Takahashi, F., Maheswaran, S., McDermott, U., Azizian, N., Zou, L., Fischbach, M.A., et al. (2010). A chromatin-mediated reversible drug-tolerant state in cancer cell subpopulations. Cell *141*, 69–80. https://doi.org/10.1016/j.cell.2010.02.027.
26. Shen, S., Vagner, S., and Robert, C. (2020). Persistent Cancer Cells: The Deadly Survivors. Cell *183*, 860–874. https://doi.org/10.1016/j.cell.2020.10.027.
27. Noronha, A., Belugali Nataraj, N., Lee, J.S., Zhitomirsky, B., Oren, Y., Oster, S., Lindzen, M., Mukherjee, S., Will, R., Ghosh, S., et al. (2022). AXL and Error-Prone DNA Replication Confer Drug Resistance and Offer Strategies to Treat EGFR-Mutant Lung Cancer. Cancer Discov. *12*, 2666–2683. https://doi.org/10.1158/2159-8290.CD-22-0111.
28. Marrocco, I., and Yarden, Y. (2023). Resistance of Lung Cancer to EGFR-Specific Kinase Inhibitors: Activation of Bypass Pathways and Endogenous Mutators. Cancers *15*, 5009. https://doi.org/10.3390/cancers15205009.
29. Mancini, M., Gaborit, N., Lindzen, M., Salame, T.M., Dall'Ora, M., Sevilla-Sharon, M., Abdul-Hai, A., Downward, J., and Yarden, Y. (2015). Combining three antibodies nullifies feedback-mediated resistance to erlotinib in lung cancer. Sci. Signal. *8*, ra53. https://doi.org/10.1126/scisignal.aaa0725.
30. Mancini, M., Gal, H., Gaborit, N., Mazzeo, L., Romaniello, D., Salame, T.M., Lindzen, M., Mahlknecht, G., Enuka, Y., Burton, D.G., et al. (2018). An oligoclonal antibody durably overcomes resistance of lung cancer to third-generation EGFR inhibitors. EMBO Mol. Med. *10*, 294–308.
31. Romaniello, D., Mazzeo, L., Mancini, M., Marrocco, I., Noronha, A., Kreitman, M., Srivastava, S., Ghosh, S., Lindzen, M., Salame, T.M., et al. (2018). A Combination of Approved Antibodies Overcomes Resistance of Lung Cancer to Osimertinib by Blocking Bypass Pathways. Clin. Cancer Res. *24*, 5610–5621.
32. Romaniello, D., Marrocco, I., Belugali Nataraj, N., Ferrer, I., Drago-Garcia, D., Vaknin, I., Oren, R., Lindzen, M., Ghosh, S., Kreitman, M., et al. (2020). Targeting HER3, a Catalytically Defective Receptor Tyrosine Kinase, Prevents Resistance of Lung Cancer to a Third-Generation EGFR Kinase Inhibitor. Cancers *12*, 2394. https://doi.org/10.3390/cancers12092394.
33. Marrocco, I., Romaniello, D., Vaknin, I., Drago-Garcia, D., Oren, R., Uribe, M.L., Belugali Nataraj, N., Ghosh, S., Eilam, R., Salame, T.M., et al. (2021). Upfront admixing antibodies and EGFR inhibitors preempts sequential treatments in lung cancer models. EMBO Mol. Med. *13*, e13144. https://doi.org/10.15252/emmm.202013144.
34. Zhou, C., Tang, K.J., Cho, B.C., Liu, B., Paz-Ares, L., Cheng, S., Kitazono, S., Thiagarajan, M., Goldman, J.W., Sabari, J.K., et al. (2023). Amivantamab plus Chemotherapy in NSCLC with EGFR Exon 20 Insertions. N. Engl. J. Med. *389*, 2039–2051. https://doi.org/10.1056/NEJMoa2306441.
35. Haga, Y., Marrocco, I., Noronha, A., Uribe, M.L., Nataraj, N.B., Sekar, A., Drago-Garcia, D., Borgoni, S., Lindzen, M., Giri, S., et al. (2021). Host-Dependent Phenotypic Resistance to EGFR Tyrosine Kinase Inhibitors. Cancer Res. *81*, 3862–3875. https://doi.org/10.1158/0008-5472.CAN-20-3555.
36. Taniguchi, H., Yamada, T., Wang, R., Tanimura, K., Adachi, Y., Nishiyama, A., Tanimoto, A., Takeuchi, S., Araujo, L.H., Boroni, M., et al. (2019). AXL confers intrinsic resistance to osimertinib and advances the emergence of tolerant cells. Nat. Commun. *10*, 259. https://doi.org/10.1038/s41467-018-08074-0.
37. Okura, N., Nishioka, N., Yamada, T., Taniguchi, H., Tanimura, K., Katayama, Y., Yoshimura, A., Watanabe, S., Kikuchi, T., Shiotsu, S., et al. (2020). ONO-7475, a Novel AXL Inhibitor, Suppresses the Adaptive Resistance to Initial EGFR-TKI Treatment in EGFR-Mutated Non-Small Cell Lung Cancer. Clin. Cancer Res. *26*, 2244–2256. https://doi.org/10.1158/1078-0432.CCR-19-2321.
38. Wang, F., Liu, X., Bartholdy, B.A., Cheng, H., and Halmos, B. (2019). Blockade of AXL activation overcomes acquired resistance to EGFR tyrosine kinase inhibition in non-small cell lung cancer. Transl. Cancer Res. *8*, 2425–2438. https://doi.org/10.21037/tcr.2019.09.61.
39. Konieczkowski, D.J., Johannessen, C.M., and Garraway, L.A. (2018). A Convergence-Based Framework for Cancer Drug Resistance. Cancer Cell *33*, 801–815. https://doi.org/10.1016/j.ccell.2018.03.025.
40. Hata, A.N., Niederst, M.J., Archibald, H.L., Gomez-Caraballo, M., Siddiqui, F.M., Mulvey, H.E., Maruvka, Y.E., Ji, F., Bhang, H.-e.C., Krishnamurthy Radhakrishna, V., et al. (2016). Tumor cells can follow distinct evolutionary paths to become resistant to epidermal growth factor receptor inhibition. Nat. Med. *22*, 262–269.
41. Faber, A.C., Corcoran, R.B., Ebi, H., Sequist, L.V., Waltman, B.A., Chung, E., Incio, J., Digumarthy, S.R., Pollack, S.F., Song, Y., et al. (2011). BIM expression in treatment-naive cancers predicts responsiveness to kinase inhibitors. Cancer Discov. *1*, 352–365.
42. Goldoni, M., and Johansson, C. (2007). A mathematical approach to study combined effects of toxicants in vitro: evaluation of the Bliss independence criterion and the Loewe additivity model. Toxicol. Vitro *21*, 759–769. https://doi.org/10.1016/j.tiv.2007.03.003.
43. Meyer, A.S., Miller, M.A., Gertler, F.B., and Lauffenburger, D.A. (2013). The receptor AXL diversifies EGFR signaling and limits the response to EGFR-targeted inhibitors in triple-negative breast cancer cells. Sci. Signal. *6*, ra66. https://doi.org/10.1126/scisignal.2004155.
44. Elkabets, M., Pazarentzos, E., Juric, D., Sheng, Q., Pelossof, R.A., Brook, S., Benzaken, A.O., Rodon, J., Morse, N., Yan, J.J., et al. (2015). AXL mediates resistance to PI3Kalpha inhibition by activating the EGFR/PKC/mTOR axis in head and neck and esophageal squamous cell carcinomas. Cancer Cell *27*, 533–546. https://doi.org/10.1016/j.ccell.2015.03.010.
45. Rogakou, E.P., Boon, C., Redon, C., and Bonner, W.M. (1999). Megabase chromatin domains involved in DNA double-strand breaks in vivo. J. Cell Biol. *146*, 905–916. https://doi.org/10.1083/jcb.146.5.905.
46. Srinivas, U.S., Tan, B.W.Q., Vellayappan, B.A., and Jeyasekharan, A.D. (2019). ROS and the DNA damage response in cancer. Redox Biol. *25*, 101084. https://doi.org/10.1016/j.redox.2018.101084.
47. Mosesson, Y., Mills, G.B., and Yarden, Y. (2008). Derailed endocytosis: an emerging feature of cancer. Nat. Rev. Cancer *8*, 835–850. https://doi.org/10.1038/nrc2521.
48. Abella, J.V., and Park, M. (2009). Breakdown of endocytosis in the oncogenic activation of receptor tyrosine kinases. Am. J. Physiol. Endocrinol. Metab. *296*, E973–E984. https://doi.org/10.1152/ajpendo.90857.2008.
49. Chew, H.Y., De Lima, P.O., Gonzalez Cruz, J.L., Banushi, B., Echejoh, G., Hu, L., Joseph, S.R., Lum, B., Rae, J., O'Donnell, J.S., et al. (2020). Endocytosis Inhibition in Humans to Improve Responses to ADCC-Mediating Antibodies. Cell *180*, 895–914.e27. https://doi.org/10.1016/j.cell.2020.02.019.
50. Isozaki, H., Sakhtemani, R., Abbasi, A., Nikpour, N., Stanzione, M., Oh, S., Langenbucher, A., Monroe, S., Su, W., Cabanos, H.F., et al. (2023). Therapy-induced APOBEC3A drives evolution of persistent cancer cells. Nature *620*, 393–401. https://doi.org/10.1038/s41586-023-06303-1.
51. Russo, M., Crisafulli, G., Sogari, A., Reilly, N.M., Arena, S., Lamba, S., Bartolini, A., Amodio, V., Magrì, A., Novara, L., et al. (2019). Adaptive mutability of colorectal cancers in response to targeted therapies. Science *366*, 1473–1480. https://doi.org/10.1126/science.aav4474.
52. Yang, W., and Gao, Y. (2018). Translesion and Repair DNA Polymerases: Diverse Structure and Mechanism. Annu. Rev. Biochem. *87*, 239–261. https://doi.org/10.1146/annurev-biochem-062917-012405.

53. Yang, Y., Gao, Y., Zlatanou, A., Tateishi, S., Yurchenko, V., Rogozin, I.B., and Vaziri, C. (2018). Diverse roles of RAD18 and Y-family DNA polymerases in tumorigenesis. Cell Cycle *17*, 833–843. https://doi.org/10.1080/15384101.2018.1456296.

54. Schaefer, W., Regula, J.T., Bähner, M., Schanzer, J., Croasdale, R., Dürr, H., Gassner, C., Georges, G., Kettenberger, H., Imhof-Jung, S., et al. (2011). Immunoglobulin domain crossover as a generic approach for the production of bispecific IgG antibodies. Proc. Natl. Acad. Sci. USA *108*, 11187–11192. https://doi.org/10.1073/pnas.1019002108.

55. Ridgway, J.B., Presta, L.G., and Carter, P. (1996). 'Knobs-into-holes' engineering of antibody CH3 domains for heavy chain heterodimerization. Protein Eng. *9*, 617–621. https://doi.org/10.1093/protein/9.7.617.

56. Sakaue-Sawano, A., Yo, M., Komatsu, N., Hiratsuka, T., Kogure, T., Hoshida, T., Goshima, N., Matsuda, M., Miyoshi, H., and Miyawaki, A. (2017). Genetically Encoded Tools for Optical Dissection of the Mammalian Cell Cycle. Mol. Cell *68*, 626–640.e5. https://doi.org/10.1016/j.molcel.2017.10.001.

57. Braun, T.P., Eide, C.A., and Druker, B.J. (2020). Response and Resistance to BCR-ABL1-Targeted Therapies. Cancer Cell *37*, 530–542. https://doi.org/10.1016/j.ccell.2020.03.006.

58. Cooper, A.J., Sequist, L.V., and Lin, J.J. (2022). Third-generation EGFR and ALK inhibitors: mechanisms of resistance and management. Nat. Rev. Clin. Oncol. *19*, 499–514. https://doi.org/10.1038/s41571-022-00639-9.

59. Marrocco, I., Romaniello, D., and Yarden, Y. (2019). Cancer Immunotherapy: The Dawn of Antibody Cocktails. Methods Mol. Biol. *1904*, 11–51.

60. Arena, S., Siravegna, G., Mussolin, B., Kearns, J.D., Wolf, B.B., Misale, S., Lazzari, L., Bertotti, A., Trusolino, L., Adjei, A.A., et al. (2016). MM-151 overcomes acquired resistance to cetuximab and panitumumab in colorectal cancers harboring EGFR extracellular domain mutations. Sci. Transl. Med. *8*, 324ra14. https://doi.org/10.1126/scitranslmed.aad5640.

61. Al-Marrawi, M.Y., Saroya, B.S., Brennan, M.C., Yang, Z., Dykes, T.M., and El-Deiry, W.S. (2013). Off-label use of cetuximab plus sorafenib and panitumumab plus regorafenib to personalize therapy for a patient with V600E BRAF-mutant metastatic colon cancer. Cancer Biol. Ther. *14*, 703–710. https://doi.org/10.4161/cbt.25191.

62. Engelman, J.A., Zejnullahu, K., Mitsudomi, T., Song, Y., Hyland, C., Park, J.O., Lindeman, N., Gale, C.-M., Zhao, X., Christensen, J., et al. (2007). MET amplification leads to gefitinib resistance in lung cancer by activating ERBB3 signaling. Science (New York, N Y) *316*, 1039–1043.

63. Lin, Z., Wang, Q., Jiang, T., Wang, W., and Zhao, J.J. (2023). Targeting tumor-associated macrophages with STING agonism improves the antitumor efficacy of osimertinib in a mouse model of EGFR-mutant lung cancer. Front. Immunol. *14*, 1077203. https://doi.org/10.3389/fimmu.2023.1077203.

64. Ferraro, D.A., Gaborit, N., Maron, R., Cohen-Dvashi, H., Porat, Z., Pareja, F., Lavi, S., Lindzen, M., Ben-Chetrit, N., Sela, M., and Yarden, Y. (2013). Inhibition of triple-negative breast cancer models by combinations of antibodies to EGFR. Proc. Natl. Acad. Sci. USA *110*, 1815–1820. https://doi.org/10.1073/pnas.1220763110.

65. Wang, C., Zhang, Y., Chen, W., Wang, Y., and Xing, D. (2023). Epidermal growth factor receptor PROTACs as an effective strategy for cancer therapy: A review. Biochim. Biophys. Acta. Rev. Cancer *1878*, 188927. https://doi.org/10.1016/j.bbcan.2023.188927.

66. Shi, S., Du, Y., Huang, L., Cui, J., Niu, J., Xu, Y., and Zhu, Q. (2022). Discovery of novel potent covalent inhibitor-based EGFR degrader with excellent in vivo efficacy. Bioorg. Chem. *120*, 105605. https://doi.org/10.1016/j.bioorg.2022.105605.

67. Stelter, P., and Ulrich, H.D. (2003). Control of spontaneous and damage-induced mutagenesis by SUMO and ubiquitin conjugation. Nature *425*, 188–191. https://doi.org/10.1038/nature01965.

68. Marrocco, I., Giri, S., Simoni-Nieves, A., Gupta, N., Rudnitsky, A., Haga, Y., Romaniello, D., Sekar, A., Zerbib, M., Oren, R., et al. (2023). L858R emerges as a potential biomarker predicting response of lung cancer models to anti-EGFR antibodies: comparison of osimertinib versus cetuximab. Cell Rep. Med. *4*, 101142.

69. Caswell, D.R., Gui, P., Mayekar, M.K., Law, E.K., Pich, O., Bailey, C., Boumelha, J., Kerr, D.L., Blakely, C.M., Manabe, T., et al. (2024). The role of APOBEC3B in lung tumor evolution and targeted cancer therapy resistance. Nat. Genet. *56*, 60–73. https://doi.org/10.1038/s41588-023-01592-8.

70. Ianevski, A., Giri, A.K., and Aittokallio, T. (2020). SynergyFinder 2.0: visual analytics of multi-drug combination synergies. Nucleic Acids Res. *48*, W488–W493. https://doi.org/10.1093/nar/gkaa216.

71. Ianevski, A., Giri, A.K., Gautam, P., Kononov, A., Potdar, S., Saarela, J., Wennerberg, K., and Aittokallio, T. (2019). Prediction of drug combination effects with a minimal set of experiments. Nat. Mach. Intell. *1*, 568–577. https://doi.org/10.1038/s42256-019-0122-4.

72. Stirling, D.R., Swain-Bowden, M.J., Lucas, A.M., Carpenter, A.E., Cimini, B.A., and Goodman, A. (2021). CellProfiler 4: improvements in speed, utility and usability. BMC Bioinf. *22*, 433. https://doi.org/10.1186/s12859-021-04344-9.

Please cite this article in press as: Simoni-Nieves et al., A bispecific antibody targeting EGFR and AXL delays resistance to osimertinib, Cell Reports Medicine (2024), https://doi.org/10.1016/j.xcrm.2024.101703

STAR★METHODS

KEY RESOURCES TABLE

REAGENT or RESOURCE	SOURCE	IDENTIFIER
Antibodies		
EGFR, Rabbit monoclonal	Cell Signaling Technology	Cat#4267; RRID:AB_2246311
pEGFR (Y1068), Rabbit polyclonal	Cell Signaling Technology	Cat#2234; RRID:AB_331701
AXL, Rabbit monoclonal	Cell Signaling Technology	Cat#8661; RRID:AB_11217435
ERK1/2, Rabbit monoclonal	Cell Signaling Technology	Cat#4695; RRID:AB_390779
pERK1/2 (Y202/204), Rabbit polyclonal	Cell Signaling Technology	Cat#9101; RRID:AB_331646
AKT1, Rabbit monoclonal	Cell Signaling Technology	Cat#2938; RRID:AB_915788
pAKT1 (S473), Rabbit monoclonal	Cell Signaling Technology	Cat#4060; RRID:AB_2315049
Caspase 3, Rabbit polyclonal	Cell Signaling Technology	Cat#9662; RRID:AB_331439
Cleaved Caspase 3 (D175), Rabbit polyclonal	Cell Signaling Technology	Cat#9661; RRID:AB_2341188
BIM, Rabbit monoclonal	Cell Signaling Technology	Cat#2933; RRID:AB_1030947
PARP1, Rabbit polyclonal	Cell Signaling Technology	Cat#95425; RRID:AB_2160739
Mcl-1, Rabbit monoclonal	Cell Signaling Technology	Cat#94296; RRID:AB_2722740
γH2AX (S139), Rabbit	Cell Signaling Technology	Cat#2577; RRID:AB_2118010
Cyclin B1, Rabbit monoclonal	Cell Signaling Technology	Cat#12231; RRID:AB_2783553
RAD18, Rabbit monoclonal	Cell Signaling Technology	Cat#9040; RRID:AB_2756446
Bak, Rabbit monoclonal	Cell Signaling Technology	Cat#12105; RRID:AB_2716685
RAD51, Rabbit monoclonal	Cell Signaling Technology	Cat#8875; RRID:AB_2721109
Ub_1-PCNA (K164), Rabbit monoclonal	Cell Signaling Technology	Cat#13439; RRID:AB_2798219
PCNA, Mouse monoclonal	Cell Signaling Technology	Cat#2586; RRID:AB_2160343
Bcl-XL, Rabbit monoclonal	Santa Cruz Technology	Cat#sc-634; RRID:AB_630917
KI67, Mouse monoclonal	Cell Signaling Technology	Cat#9449; RRID:AB_2797703
DNA Pol iota, Mouse polyclonal	Santa Cruz Technology	Cat#sc-101026; RRID:AB_2167019
GAPDH, Mouse monoclonal	Millipore	Cat#MAB374; RRID:AB_2107445
Vinculin, Mouse monoclonal	Sigma-Aldrich	Cat#V9264; RRID:AB_10603627
Pol η, Rabbit polyclonal	Abcam	Cat#ab234855
Pol κ, Rabbit polyclonal	Abcam	Cat#ab86076; RRID:AB_1925334
MLH1, Rabbit monoclonal	Abcam	Cat#ab92312; RRID:AB_2049968
MSH2, Rabbit monoclonal	Abcam	Cat#ab92473; RRID:AB_10585291
Anti-mouse Alexa Fluor 488-conjugated secondary antibody	Thermo Fisher Scientific	Cat#A-31570; RRID:AB_2536180
Anti-rabbit Alexa Fluor 555-conjugated secondary antibody	Thermo Fisher Scientific	Cat#A-31572; RRID:AB_162543
141Pr conjugated APC anti-human CD326 (EpCAM)	BioLegend	Cat# 324208; RRID:AB_756082
89Y conjugated Purified anti-human CD45	BioLegend	Cat#304002; RRID:AB_314390
Biological samples		
Patient derived xenograft (PDX) TM00193	The Jackson Laboratory	TM00193
Chemicals, peptides, and recombinant proteins		
Erlotinib	LC Laboratories	Cat#E−4997
Osimertinib	Gift from AstraZeneca	N/A
Cetuximab (Erbitux®)	Merck	N/A
NAC (N-acetyl-L-cysteine)	Sigma-Aldrich	Cat# A9165; CAS: 616-91-1
DCFDA (2',7'-Dichlorofluorescin Diacetate)	Thermo Fisher Scientific	Cat#D399
Triton X-100	Sigma-Aldrich	Cat#T8787; CAS: 9036-19-5

(*Continued on next page*)

Continued

REAGENT or RESOURCE	SOURCE	IDENTIFIER
MTT (3-(4,5-dimethylthiazol-2-yl)-2, 5-diphenyltetrazolium bromide)	Sigma-Aldrich	Cat#M5655; CAS: 298-93-1
FITC-labeled phalloidin	Sigma-Aldrich	Cat#P5282
Cisplatin 194Pt	Standard Biotools	Cat#201194
Iridium	Standard Biotools	Cat#201192A
Palladium	Standard Biotools	Cat#201060
Critical commercial assays		
FuGENE HD Transfection Reagent	Promega	Cat#E2311
Cell Titer 96 One Solution Proliferation Assay	Promega	Cat#G3580
Experimental models: Cell lines		
PC9	Gift from Julian Downward, Francis Crick Institute, London	RRID:CVCL_B260
H1975	ATCC	Cat# CRL-5908; RRID:CVCL_1511
HEK293T	ATCC	Cat# CRL-3216; RRID:CVCL_0063
Experimental models: Organisms/strains		
CD1 nude mice (HsdHli:CD1-Foxn1nu)	Envigo Israel	N/A
NSG mice	The Jackson Laboratory	RRID:IMSR_JAX:005557
Recombinant DNA		
Fucci(CA)2/pCSII-EF	RIKEN BRC	RDB15446
psPAX2	Addgene	Plasmid #12260
pMD2.G	Addgene	Plasmid #12259
Software and algorithms		
GraphPad Prism v9.0.2	GraphPad Software	RRID:SCR_002798
ImageJ v1.53t	National Institute of Health (NIH)	RRID:SCR_003070
Cell Profiler v4.2.1	Broad Institute	RRID:SCR_007358
Image Lab v6.0.1	Bio-Rad	RRID:SCR_014210
ReViSP v2.3	Piccinini et al.[59] Piccinini et al.[60]	N/A
R v4.2.1	The R Foundation	RRID:SCR_001905

EXPERIMENTAL MODEL AND STUDY PARTICIPANT DETAILS

Cell cultures

PC9 cells (EGFR-mutated human NSCLC cells) were a gift from Julian Downward (Francis Crick Institute, London, UK). Cells were cultured at 37°C under 5% CO_2 in RPMI medium supplemented with 10% fetal bovine serum (FBS) and antibiotics. Cell treatments included the following drugs: osimertinib (a gift from AstraZeneca), cetuximab (Merck KGaA), mAb654 (generated in our lab[27]) and Bis1 (generated in this study).

Animal studies

All animal studies were approved by our institutional board and they were performed in accordance with the guidelines of the Institutional Animal Care and Use Committee (IACUC). PC9 cells ($3X10^6$ cells per mouse), were subcutaneously injected in the right flanks of 6-weeks old CD1 nude mice. Once tumors reached a volume of approximately 500 mm^3, mice were randomized into different groups and treated as indicated. TKIs were daily administered using oral gavage. Antibodies were administered twice a week using intraperitoneal injection at a final dose of 0.2 mg/mouse/injection. The TM00193 (exon 19 deletion) PDX model was purchased from the Jackson Laboratory and implanted in NSG mice. Following euthanasia, tumors were removed from donor mice and cut into small fragments. A small pouch was made in the lower back of each mouse, and one fragment was later inserted into the pouch. The wound was closed using a surgical clip. Clips were removed 4–5 days after surgery. Treatments started when tumors reached a volume of approximately 350 mm^3. Mice were labeled with RF identification chips (from Troven). Tumors were measured twice a week with a caliper, and body weight was measured once a week. Tumor volume was calculated by using the formula (T1*T2*(T1+T2)/2)/2. Mice were euthanized when tumors reached approximately 1500 mm^3.

CellPress
OPEN ACCESS

Cell Reports Medicine
Article

METHOD DETAILS

Cell viability assays

Cell viability was assessed using MTT (3-(4,5-dimethylthiazol-2-yl)-2,5-diphenyltetrazolium bromide). PC9 cells ($3x10^3$/well) were seeded in 96-well plates and the day after, they were treated for 72 h with the indicated drugs. Afterward, cells were incubated for 3 h at 37°C with the MTT solution (0.5 mg/mL), followed by solubilization of the formazan crystals in DMSO. Absorbance was read at 570 nm.

Cell proliferation assays

Cells were seeded in 96-well plates (1000 cells per well), and on the next day, they were treated for 1, 3, 5, or 7 days with the indicated drugs. At each time point, proliferation was addressed by CellTiter Cell Proliferation assay (Promega). To detect cell growth, light absorbance (490 nM) was determined using a microplate reader.

Immunofluorescence analysis

Following treatments, cells were washed in saline and fixed in 4% paraformaldehyde for 15 min at room temperature. Afterward, cells were permeabilized for 10 min in saline containing 0.2% Triton X-100 and blocked for 65 min in 1% bovine serum albumin, followed by hybridization with a primary antibody (Ki67 or gamma-H2AX). On the next day, cells were washed and incubated for 1 h in the dark with an anti-mouse or anti-rabbit Alexa Fluor 488-conjugated secondary antibody, along with DAPI and Rhodamine B labeled phalloidin. Images were captured using a Zeiss Spinning Disk confocal microscope and processed using the Zeiss ZEN 3.1 and ImageJ applications.

Colony formation assays

Cells were seeded in 6-well plates at a density of 1000 cells per well, and on the next day they were treated as indicated in the figure legends. Media (with drugs) were refreshed once every 3 days. Following 14-day-long treatments, cells were washed, fixed for 20 min in ice-cold methanol, and then stained for 15 min at room temperature with 2% crystal violet. Full well photos were captured using an Epson Perfection 4870 Photo Scanner (Long Beach, CA, USA). For signal quantification, images corresponding to 5 non-overlapping fields were taken with a light microscope (Olympus Corporation, Tokyo, Japan) and quantified using ImageJ.

Immunoblotting and ELISA assays

Protein extracts were obtained by treating cells with lysis buffer (50 mM TRIS pH 7.5, 150 mM NaCl, 1% Nonidet P-40, 0.5% sodium deoxycholate, 1 mM EDTA, 0.1 mM sodium orthovanadate and a complete protease inhibitor cocktail), and resolved using electrophoresis, followed by transfer to a nitrocellulose membrane. Afterward, membranes were blocked for 1 h at room temperature and incubated overnight with the indicated primary antibodies, followed by incubation (1 h) with horseradish peroxidase- (HRP-) conjugated secondary antibodies. Bands were detected using the Clarity Western ECL Blotting Substrates (Bio-Rad) and the ChemiDoc Imaging System (Bio-Rad). Images were acquired using the ImageLab Software (Bio-Rad). To validate simultaneous binding of Bis1 to AXL and EGFR, we performed a sandwich ELISA test that used a recombinant form of AXL (extracellular domain) and a biotinylated soluble form of EGFR. Firstly, the ELISA plate was coated overnight with the AXL protein (2 μg/mL), and later the washed plate was incubated for 2 h with increasing concentrations of Bis1 (0–150 μg/mL). Next, we added the biotinylated soluble form of EGFR, and this was followed by a short incubation with an Avidin-HRP and a development reaction.

ROS production assays

PC9 cells were seeded in 6-well plates and on the next day, they were treated with the indicated drugs for 6 h. Hydrogen peroxide levels were assessed by incubating cells with 2',7'-dichlorofluorescin diacetate (DCFDA; 10 mM, diluted in Krebs-Ringer phosphate buffer) for 30 min in the dark at 37°C and under 5% CO_2. After washing the cells twice in Krebs-Ringer phosphate buffer, cellular fluorescence was recorded using epifluorescence microscopy (Olympus Corporation, Japan) at a wavelength of 500 nm (excitation) and 580 nm (emission). Signals were quantified using ImageJ.

RNA isolation and real-time PCR

Total RNA was extracted using the RNeasy Mini Kit (QIAGEN) according to the manufacturer's instructions. Complementary cDNA was synthesized using the qScript cDNA synthesis kit (Quantabio). Real time quantitative PCR (RT-PCR) analyses were performed using SYBR green (Applied Biosystem) and specific primers (see complete list of primers in Table S1) on the StepOne Plus Real-Time PCR system (Applied Biosystems). RT-PCR signals (Ct) were normalized to GAPDH.

Surface plasmon resonance (SPR) measurements

The formation and dissociation of antigen-antibody complexes were monitored by surface plasmon resonance using BIAcore 200. Antibodies were immobilized on CM5 chips as described below. HBS-EP buffer (10 mM HEPES with 0.15 M NaCl, 3 mM EDTA, and 0.05% surfactant P20 at pH 7.4) was used as the running buffer. After activation for 7.5 min (flow rate 10 μL/min) with a freshly prepared mixture of N-hydroxysuccinimide (50 mM in water) and 1-ethyl-3-(3-dimethylaminopropyl) carbodiimide (195 mM in water),

antibodies (2.5 μg/mL in 150 mM sodium acetate buffer, pH 4.6) were injected for 5 min (flow rate: 10 μL/min) to reach 1300 RU. Carboxylic groups that remained activated were blocked by injecting ethanolamine hydrochloride (1 M), pH 8.6 (for 5 min; flow rate: 10 μL/min). A total of 1300 RU of the antibody were immobilized using this method. The association of the soluble receptor, either AXL or EGFR, with the respective antibody was monitored by injecting different concentrations of the soluble receptor for 5 min at a flow rate of 30 μL/min. The dissociation of the soluble receptor from an antibody was followed by stopping injection. NaOH (5 mM) was employed while regenerating the chip. For data analysis, sensograms were fitted to a steady state model (T200 software). All experiments involved at least 2 independent biological repeats.

Drug synergy analysis

The expected drug combination responses were calculated based on the Bliss reference model using SynergyFinder (https://github.com/IanevskiAleksandr/SynergyFinder#readme). Deviations between the observed and the expected responses with positive and negative values denote synergy and antagonism, respectively.[70] For the estimation of outlier measurements we utilized the cNMF (composite non-Negative Matrix Factorization) algorithm.[71]

Design and expression of recombinant antibodies

The cDNA encoding the variable heavy and light domains of cetuximab, the anti-human EGFR antibody, were synthesized based on their published sequences. Similarly, the variable heavy and light regions of mAb654, a murine anti-human AXL antibody, were sequenced from the respective hybridoma. The variable region encoding DNA sequences of each parental antibody were inserted into mammalian expression vectors corresponding to human IgG1 or human kappa Fc backbones. Alternatively, we utilized a vector suitable for construction of bi-specific antibodies. For correct heavy–light chain pairing, the parental EGFR-targeting arm was expressed in the CrossMab format (CH1-CL swapping). For the AXL-targeting arm, the wildtype domain architecture was maintained. For heavy chain heterodimerization, the following point mutations were introduced in the CH3 domain: Y349C/T366S/L368A/Y407V in the EGFR-targeting arm and S354C/T366W in the AXL-targeting arm. The mutated plasmid sequences were validated by means of direct sequencing (Life Science Core Facility, Weizmann Institute of Science). For antibody production, heavy and light chain expression vectors were transiently transfected into Expi293 cells (ThermoFisher). Secreted antibodies in the supernatant were purified using protein G Sepharose 4 Fast Flow (GE Healthcare), dialyzed against phosphate-buffered saline and sterile filtered (0.22 μm). Purity was assessed using SDS–polyacrylamide gel electrophoresis and Coomassie Blue staining, and was estimated to be >90%. Size-exclusion chromatography was performed using a Superose 6 Increase 10/300GL column (GE Healthcare) on an Äkta Pure 25 FPLC system.

Cell cycle distribution using Fucci

The ubiquitination-based cell cycle indicator (Fucci),[56] which enables real-time monitoring of interphase and cell-cycle progression, was employed using PC9 cells. Lentiviruses were packaged by using the Fugene HD reagent (Promega) and co-transfecting HEK293T cells with Fucci(CA)2/pCSII-EF (RIKEN BRC, Tsukuba, Japan), psPAX2 (Addgene, #12260) and pMD2.G (Addgene #12259). PC9 cells were infected with virus and single cell clones were obtained by means of serial dilution. A high-content imaging system (CV8000, from Yokogawa) was used to capture cellular images. Fluorescent, virus transduced cells were treated in the absence or presence of drugs, which were refreshed once every three days. A high-content imaging system (CV8000, from Yokogawa) was used to capture cellular images. The fluorescence intensity of green and red signals was used to determine the proliferating fraction of cells (S-phase), arrested cells (G1-phase) and other fractions (G2-M). Analysis was performed using CellProfiler[72] and the R software.

Spheroid assays

H1975 ($1.5x10^4$) or PC9 cells ($5x10^3$) cells were grown in suspension over a 0.6% agar layer diluted in full medium supplemented with the indicated drugs. Non-overlapping fields of each well were photographed after 8–10 days using the OpTech IB4 microscope. Flat cell layers were analyzed for the percentage of covered area using the ImageJ software. For assays performed in Matrigel, 96-well plates were pre-coated with basement membrane extract (BME; 80%) and incubated for 30 min at 37°C. Thereafter, cells ($1x10^3$) were layered on top of the gelled BME and cultured in 5% BME diluted in drug-containing medium. Experiments were stopped after 6–7 days and pictures were captured and analyzed as above.

ADCC assays

PC9 cells ($2x10^4$) were co-cultured with PBMCs ($1x10^6$ cells, from ATCC) and subjected to blocking Fc-receptors using a solution from BD Biosciences and surface staining using the anti-human CD326/EpCAM (9C4) antibody from Fluidigm. For viability determination, we incubated samples with cisplatin (194Pt/195Pt/196pt/198Pt; 1.25mM) followed by deactivation in complete RPMI medium. Samples were barcoded after suspending them in Maxpar nuclear antigen staining buffer and fixation that utilized Maxpar Fix I and the Maxpar Barcode Perm Buffer. Cell ID Palladium barcoding was done for each sample prior to pooling all samples in one tube. The final fixation of the pooled sample was performed using freshly made paraformaldehyde (PFA; 4%). Cells were further stained using Cell ID Intercalator-Ir-125 nM (Iridium solution at 250 nM). Each sample was washed thoroughly and suspended in Maxpar Cell Acquisition Solution Plus (CAS+). CyTOF EQ Four Element Calibration beads (1:10, EQ Beads) were resuspended in

CAS+ solution. Cells in the sample were counted and gravity filtration was done thrice to remove clumps and debris using 35-μm filter mesh cell strainer (Falcon). The CyTOF- Helios mass cytometer (Fluidigm) was employed, along with cells ($2x10^6$ per mL) and beads. The resulting data were pre-processed to normalize and concatenate prior to analysis that made use of CyTOF Software v.6.7.1014. Gates were applied using the Cytobank platform (Beckman Coulter). The normalized beads were gated out and then live and dead cells were gated using cisplatin-194Pt and Iridium DNA label 193Ir. Event length and Gaussian parameters considering the width, center, offset and residual channels were used. CyTOF software was then used for sample de-barcoding. The debarcoded dataset was analyzed using FlowJo to determine the dead cell population. The calculation of ADCC activity was performed using the formula [% Specific Cell Death (%EpCAM+/Cisplatin 194Pt) – (% spontaneous cell death)/100 – (% spontaneous cell death)] * 100.

QUANTIFICATION AND STATISTICAL ANALYSIS

The GraphPad Prism (version 8.0.2) software was used to perform statistical analyses. Sample numbers and other information (mean ± SEM, number of replicates and specific statistical tests) are indicated in the respective figure legends. We employed one-way ANOVA and Dunnett's multiple comparison test. Differences were considered statistically significant when $p < 0.05$. p values are shown as follows: *, $p < 0.05$; **, $p < 0.01$; ***, $p < 0.005$; ****, $p < 0.001$. The ImageJ and Image Lab software packages were used to perform data analyses.